EUROPEAN HEMATOLOGY ASSOCIATION
haematologica
Journal of the European Hematology Association

# Sphingolipid dysregulation due to lack of functional KDSR impairs proplatelet formation causing thrombocytopenia

by Tadbir K Bariana, Veerle Labarque, Jessica Heremans, Chantal Thys, Mara De Reys, Daniel Greene, Benjamin Jenkins, Luigi Grassi, Denis Seyres, Frances Burden, Deborah Whitehorn, Olga Shamardina, Sofia Papadia, Keith Gomez, NIHR BioResource, Chris Van Geet, Albert Koulman, Willem H Ouwehand, Cedric Ghevaert, Mattia Frontini, Ernest Turro, and Kathleen Freson. Collaborative Groups: NIHR BioResource (Jayanthi Alamelu, Raza Alikhan, David Allsup, Arif Alvi, Steve Austin, Trevor Baglin, Tamam Bakchoul, Gareth Baynam, Neha Bhatnagar, Tina Biss, Sara Boyce, Elizabeth Chalmers, Melissa V Chan, Janine Collins, Peter W Collins, Nicola S Curry, Kate Downes, Tina Dutt, Wendy N Erber, Gillian Evans, Tamara Everington, Remi Favier, Bruce Furie, Michael Gattens, Greinacher Andreas, Gresele Paolo, Daniel Hart, Yvonne M C Henskens, Rashid Kazmi, David Keeling, Anne M Kelly, Michael A Laffan, Michele Lambert, Claire Lentaigne, Ri Liesner, Bella Madan, Mike Makris, Carolyn Millar, Andrew D Mumford, Sarah Mangles, Mary Mathias, Paquita Nurden, Samya Obaji, K John Pasi, Jeanette H Payne, Kathelijne Peerlinck, Fernando Pinto, Shoshana Revel-Vilk, Sylvia Richardson, Mike Richards, Matthew T Rondina, Catherine Roughley, Sol Schulman, Harald Schulze, Suthesh Sivapalaratnam, Ilenia Simeoni, Marie Scully, Susan E Shapiro, Keith Sibson, Matthew C Sims, Matthew J Stubbs, R Campbell Tait, Kate Talks, Gordon B Taylor, Jecko Thachil, Cheng-Hock Toh, Minka J A Vries, Timothy Warner, Henry G Watson, Sarah K Westbury, John-Paul Westwood)

Haematologica 2018 [Epub ahead of print]

*Citation: Tadbir K Bariana, Veerle Labarque, Jessica Heremans, Chantal Thys, Mara De Reys, Daniel Greene, Benjamin Jenkins, Luigi Grassi, Denis Seyres, Frances Burden, Deborah Whitehorn, Olga Shamardina, Sofia Papadia, Keith Gomez, NIHR BioResource, Chris Van Geet, Albert Koulman, Willem H Ouwehand, Cedric Ghevaert, Mattia Frontini, Ernest Turro, and Kathleen Freson. Collaborative Groups: NIHR BioResource (Jayanthi Alamelu, Raza Alikhan, David Allsup, Arif Alvi, Steve Austin, Trevor Baglin, Tamam Bakchoul, Gareth Baynam, Neha Bhatnagar, Tina Biss, Sara Boyce, Elizabeth Chalmers, Melissa V Chan, Janine Collins, Peter W Collins, Nicola S Curry, Kate Downes, Tina Dutt, Wendy N Erber, Gillian Evans, Tamara Everington, Remi Favier, Bruce Furie, Michael Gattens, Greinacher Andreas, Gresele Paolo, Daniel Hart, Yvonne M C Henskens, Rashid Kazmi, David Keeling, Anne M Kelly, Michael A Laffan, Michele Lambert, Claire Lentaigne, Ri Liesner, Bella Madan, Mike Makris, Carolyn Millar, Andrew D Mumford, Sarah Mangles, Mary Mathias, Paquita Nurden, Samya Obaji, K John Pasi, Jeanette H Payne, Kathelijne Peerlinck, Fernando Pinto, Shoshana Revel-Vilk, Sylvia Richardson, Mike Richards, Matthew T Rondina, Catherine Roughley, Sol Schulman, Harald Schulze, Suthesh Sivapalaratnam, Ilenia Simeoni, Marie Scully, Susan E Shapiro, Keith Sibson, Matthew C Sims, Matthew J Stubbs, R Campbell Tait, Kate Talks, Gordon B Taylor, Jecko Thachil, Cheng-Hock Toh, Minka J A Vries, Timothy Warner, Henry G Watson, Sarah K Westbury, John-Paul Westwood). Sphingolipid dysregulation due to lack of functional KDSR impairs proplatelet formation causing thrombocytopenia.*
*Haematologica. 2018; 103:xxx*
*doi:10.3324/haematol.2018.204784*

**Sphingolipid dysregulation due to lack of functional *KDSR* impairs proplatelet formation causing thrombocytopenia**

Scientific category: Platelets and Thrombopoiesis

Short title for running head: *Mechanism of KDSR-associated thrombocytopenia*

Tadbir K Bariana[1-3,4], Veerle Labarque[5], Jessica Heremans[5], Chantal Thys[4,5], Mara De Reys[5], Daniel Greene[3,4,6,7], Benjamin Jenkins[8], Luigi Grassi[3,4,6,7], Denis Seyres[3,4,6,7], Frances Burden[3,4,6], Deborah Whitehorn[3,4,6], Olga Shamardina[3,4,6], Sofia Papadia[3,4,6], Keith Gomez[1,2,4], NIHR BioResource[4], Chris Van Geet[4,5], Albert Koulman[8], Willem H Ouwehand[3,4,6,9,10], Cedric Ghevaert[3,6,9], Mattia Frontini[3,4,6,9], Ernest Turro[3,4,6,7], Kathleen Freson[4,5]

[1]Department of Haematology, University College London, London, United Kingdom

[2]The Katharine Dormandy Haemophilia Centre and Thrombosis Unit, Royal Free London NHS Foundation Trust, London, United Kingdom

[3]Department of Haematology, University of Cambridge, Cambridge Biomedical Campus, Cambridge, United Kingdom

[4]NIHR BioResource, Cambridge University Hospitals, Cambridge Biomedical Campus, Cambridge, United Kingdom

[5]Department of Cardiovascular Sciences, Center for Molecular and Vascular Biology, University of Leuven, Belgium

[6]NHS Blood and Transplant, Cambridge Biomedical Campus, Cambridge, United Kingdom

[7]Medical Research Council Biostatistics Unit, Cambridge Institute of Public Health, Cambridge Biomedical Campus, Cambridge, United Kingdom

[8]NIHR Biomedical Research Centre Core Metabolomics and Lipidomics Laboratory, University of Cambridge, Cambridge Biomedical Campus, Cambridge, United Kingdom

[9]British Heart Foundation Centre of Excellence, Division of Cardiovascular Medicine, Cambridge University Hospitals, Cambridge Biomedical Campus, Cambridge, United Kingdom

[10]Wellcome Sanger Institute, Wellcome Genome Campus, Hinxton, Cambridge, United Kingdom

Correspondence to

Kathleen Freson

Department of Cardiovascular Science

Center for Molecular and Vascular Biology

Herestraat 49, 3000 Leuven, Belgium

kathleen.freson@med.kuleuven.be

Abstract word count: 249

Text word count: 3009

6 figures, 1 supplemental file

**Abstract**

Sphingolipids are fundamental to membrane trafficking, apoptosis and cell differentiation and proliferation. KDSR or 3-keto-dihydrosphingosine reductase is an essential enzyme for *de novo* sphingolipid synthesis, and pathogenic mutations in *KDSR* result in the severe skin disorder *erythrokeratodermia variabilis et progressiva-4*. Four of the eight reported cases also had thrombocytopenia but the underlying mechanism has remained unexplored. Here we expand upon the phenotypic spectrum of KDSR deficiency with studies in two siblings with novel compound heterozygous variants associated with thrombocytopenia, anemia and minimal skin involvement. We report a novel phenotype of progressive juvenile myelofibrosis in the propositus, with spontaneous recovery of anemia and thrombocytopenia in the first decade of life. Examination of bone marrow biopsies showed megakaryocyte hyperproliferation and dysplasia. Megakaryocytes obtained by culture of $CD34^+$ stem cells confirmed hyperproliferation and showed reduced proplatelet formation. The effect of KDSR insufficiency on the sphingolipid profile was unknown, and was explored *in vivo* and *in vitro* by a broad metabolomics screen that indicated activation of an *in vivo* compensatory pathway that leads to normalisation of downstream metabolites such as ceramide. Differentiation of propositus-derived induced pluripotent stem cells to megakaryocytes followed by expression of functional KDSR showed correction of the aberrant cellular and biochemical phenotypes, corroborating the critical role of *KDSR* in proplatelet formation. Finally, Kdsr depletion in zebrafish recapitulated the thrombocytopenia and showed biochemical changes similar to those observed in the affected siblings. These studies support an important role for sphingolipids as regulators of cytoskeletal organisation during megakaryopoiesis and proplatelet formation.

## Introduction

KDSR or 3-keto-dihydrosphingosine reductase is an early, essential enzyme in the pathway of *de novo* sphingolipid synthesis that catalyzes the conversion of 3-keto-dihydrosphingosine (KDS) to dihydrosphingosine (DHS) on the cytosolic leaflet of the endoplasmic reticulum.[1] The canonical transcript for *KDSR* encodes a 332 amino acid protein. The gene is widely transcribed,[1-3] consistent with the integral roles of the sphingolipid family in forming lipid rafts that facilitate membrane trafficking and in the regulation of fundamental cellular functions that include apoptosis, differentiation, and proliferation.[4] The importance of sphingolipid synthesis for normal cellular functions is illustrated by the complex multisystem phenotypes of null mice for key enzymes or receptors in the pathway, including defective platelet activation and thrombus formation.[5, 6] A pathway for *de novo* synthesis of sphingolipids in a megakaryocytic cell line has been shown, but plays a minimal role in mature platelets, which instead acquire essential sphingolipids by incorporating them from plasma or recycling plasma membrane sphingomyelins, both largely independently of KDSR.[7]

Consistent with these important roles of sphingolipids, compound heterozygous variants in *KDSR* (Figure 1) have recently been identified as causal of the severe skin disorder *erythrokeratodermia variabilis et progressiva 4* (EKVP4, OMIM617526), a condition characterised by neonatal onset of thick, scaly skin on the face and genitals and milder erythematous palmo-plantar scaling.[8] This observation established a role for *KDSR* in the homeostasis of keratinisation, however it was unclear whether these cases had hematological pathologies. A more recent study described four probands with EKVP4 caused by *KDSR* variants accompanied by severe thrombocytopenia and platelet dysfunction in infancy.[9] A reduction in plasma S1P and surface-exposed ceramide in human platelets, as well as diminished ceramide levels in affected skin were reported. Bone marrow morphology in one patient was normal and in a second one demonstrated increased megakaryopoiesis. For this patient a diagnosis of immune-mediated thrombocytopenia was made with no response to corticosteroid treatment and minimal response to splenectomy. No further exploration of the molecular mechanism underlying the thrombocytopenia was undertaken.[9]

Here we provide evidence that in this pedigree, *KDSR* plays a fundamental role in megakaryopoiesis, cytoplasmic organisation and proplatelet formation. We describe a pedigree in which compound heterozygous variants in *KDSR* segregate with severe thrombocytopenia and minimal or no skin involvement. We report novel phenotypes of progressive juvenile myelofibrosis in the propositus, who is older, and anemia in both siblings. Broad metabolic profiling complemented by targeted mass spectrometry assays confirm KDSR hypofunction and suggest activation of an alternative, compensatory pathway *in vivo*. Depletion of *kdsr* in zebrafish and studies with $CD34^+$ stem cell- and induced pluripotent stem cell (iPSC)-derived MK show cellular and biochemical signatures in common with those observed in our patients, showing the mechanism by which *KDSR* variants mediate thrombocytopenia.

## Methods

*Recruitment and sequencing*

Following informed, written consent (ethical study approval ML3580), the propositus was recruited to the Bleeding, thrombotic and Platelet Disorders (BPD) domain of the NIHR BioResource-Rare Diseases study (UK Research Ethics Committee 13/EE/0325, https://bioresource.nihr.ac.uk). Further details are provided in the supplemental Methods.

*Platelet studies*

Aggregation and transmission electron microscopy (EM) studies were performed as described previously.[10]

*Metabolic profiling*

Global metabolic profiling of plasma was performed by Metabolon, Inc. (Durham, NC) using the DiscoveryHD4 liquid chromatography tandem mass spectrometry (LC-MS/MS) platform, as previously described.[11] Results of study participants were

compared with 496 subjects between the ages of 4 and 55 years without thrombocytopenia. A separate LC-MS platform method, previously described,[12, 13] was used for specific confirmation of the global sphingolipid profile. Further details are provided in the supplemental Methods.

*Stem cell differentiation assays*

$CD34^+$ hematopoietic stem cells (HSC) were isolated by magnetic cell sorting (Miltenyi Biotec, Bergisch Gladback, DE) from bone marrow aspirates from the propositus (at 5 years of age) and an unrelated control, and from peripheral blood from the propositus (at 8·5 years of age), his affected sister (at 5 months of age) and an unrelated control.

In addition, expanded bone marrow- and peripheral blood- derived HSC at day 3 of differentiation were used for liquid MK cultures in two experiments. In the first experiment, HSC obtained from the bone marrow of the propositus were differentiated in parallel to a control. For the second experiment, HSC obtained from the peripheral blood of the propositus and his affected sister were cultured in parallel with a different control. Details of the differentiation protocols, colony assays and statistical analysis of MK immunostaining are provided in the supplemental Methods.

*Zebrafish analysis*

Tg(cd41:EGF) embryos[14] were injected at the one-cell stage with a *kdsr* ATG morpholino (MO) (5' ctcagaggacatgggtcaacctgat, Kdsr-MO) purchased from Gene Tools LLC (Philomath, OR) or with buffer (control). Zebrafish *kdsr* has ZFIN accession number ZDB-GENE-040426-853. Thrombocyte formation was analysed as described previously.[15, 16] Immunoblots were developed with goat anti-GFP (Rockland) and anti-FVT1/KDSR (Clone H-149; Santa Cruz). All animal protocols were approved by the Ethical Committee of KU Leuven.

*Lentiviral reference KDSR transcript expression in iPSC*

iPSC were prepared by the Cambridge Biomedical Research Centre iPSC core laboratory as described in the supplemental Methods. iPSC were transduced with the lentiviral vector to express the open reading frame (ORF) of *KDSR* (pLenti-EF1a-KDSR-myc-DDK-IRES-Puro, Origene) and the un-cloned destination vector PS10085 (Origene) to generate the reference transcript rescue line ($K^{resc}$) and empty vector control line ($K^{ev}$), respectively. The ORF is identical to transcript ENST00000591902 (RefSeq accession no. NM_002035, Origene TrueClone cDNA cat. RC201153), which has the highest reported expression in MK.[2] Details of lentiviral particle production, transduction and selection are given in the supplemental Methods.

*Forward programming to MK (iMK)*

iPSC were reprogrammed to MK (named iMK hereafter) using a protocol for generating MK described by Moreau *et al*.[17] $K^{resc}$ and $K^{ev}$ iMK were generated in three independent experiments. Details of iMK reprogramming, immunophenotyping, the proplatelet assay and RNA sequencing are given in the supplemental Methods.

**Results**

*Clinical characteristics*

The eight-year old male propositus was born to healthy, unrelated parents of European ancestry (Figure 2A). At 4 months of age he presented with a viral infection and was found to have a platelet count of $65x10^9$/L and mild normocytic, normochromic anemia with normal iron and hematinic levels (Figure 2B, supplemental Table 1A, supplemental Figure 1). Subsequent complete blood counts showed on several occasions platelet counts $<100x10^9$/L accompanied by rectal and gingival bleeding, excessive ecchymosis, and recurrent epistaxis when platelet counts were $<10x10^9$/L. Possible skin involvement was limited to a slow-to-heal perianal wound following rectal manometry. Serial bone marrow examinations revealed increased numbers of dysplastic MK and progressive severe myelofibrosis (Figure 2C, supplemental Figure 2, supplemental Table 1B); despite this we observed significant

fluctuation in the propositus' thrombocytopenia and normalisation of the hemoglobin level over the course of his first decade (Figure 2B, supplemental Table 1A). The mechanism of the improvement is unclear, and occurred in the absence of identifiable environmental, therapeutic, or dietary interventions. Genetic analyses of bone marrow DNA excluded known somatic mutations causal of myelodysplasia or primary myelofibrosis (supplemental Table 1B). Light transmission platelet aggregation was normal with the exception of an attenuated response to stimulation with collagen at low dose (supplemental Table 1C). The propositus' older brother and his parents were unaffected (Figure 2A). His sister presented at birth with thrombocytopenia (Figure 2A and B, supplemental Table 1A) and mild ichthyosis in her left axilla (Figure 2D), but the skin symptoms resolved spontaneously over the first month. At 5 months of age she also developed persistent, normocytic, normochromic anemia (Figure 2B, supplemental Table 1A). Transmission EM analysis showed platelets of normal size (Figure 2E). Delta-granules appeared diminished, however it was not possible to count these accurately in the absence of whole-mount EM or a specific δ-granule marker (CD63 also stains lysosomal structures). There were no other marked ultrastructural abnormalities.

*Pathogenic variants in KDSR*

The propositus and his affected sister carry a maternally inherited nonsense variant 18:61006104 G>A (p.Arg236*) and a paternally inherited missense variant 18:61018270 G>A (p.Arg154Trp) in *KDSR* (Figure 2A). The variants were confirmed by Sanger sequencing (supplemental Figure 3) and have minor allele frequencies in Europeans of $4{\cdot}82x10^{-5}$ and $2{\cdot}32x10^{-4}$ respectively.[18, 19] The missense variant p.Arg154Trp is localised in the catalytic domain of KDSR (Figure 1)[20] and both are found in the most abundant *KDSR* transcripts in MK (supplemental Figure 4).[2] The nonsense variant is absent from two out of three major platelet transcripts, which is in keeping with minimal *de novo* sphingolipid synthesis in mature platelets (supplemental Figure 4).[7] The results of co-segregation study were concordant with an autosomal recessive mode of inheritance (Figure 2A).

*Sphingolipid profiles*

We reasoned that the variants would cause reduced enzymatic function, leading to a build-up of the substrate KDS (Figure 3A). Indeed global metabolic profiling showed KDS to be detectable in plasma from the propositus but not from the parents, the healthy sibling, and 496 unrelated controls (Figure 3B). This finding was corroborated using a LC-MS platform for the selective measurement of specific sphingolipids, which confirmed that KDS was detectable in both patients and absent from the plasma of controls (Figure 3C, supplemental Figure 5). Interestingly, there was no reduction in downstream sphingolipids in the patients using either platform (supplemental Tables 2 and 3A). In fact, global profiling showed levels of the KDSR product, DHS, were higher for the propositus than controls. These findings raise the hypothesis that KDSR hypofunction during *de novo* sphingolipid synthesis is compensated *in vivo* by alternative mechanisms, for example by the recycling of relatively abundant sphingomyelins along a pathway that normally contributes little to free DHS production.[4]

*Depletion of kdsr in zebrafish causes thrombocytopenia*

We explored the role of the enzyme on thrombocyte formation in zebrafish by MO-mediated depletion of the *kdsr* transcript in Tg(cd41:EGFP). This led as expected to a reduction of the Kdsr protein level (Figure 4A and B) and resulted in curved tails, which is a typical feature for embryos with thrombocytopenia (supplemental Figure 6).[15] The number of thrombocytes was inversely correlated with the dose of MO injected (Figure 4C and D). Targeted sphingolipid profiling showed elevated and undetectable KDS in lysates from MO and control embryos, respectively (Figure 4E). Similar to the results obtained with the propositus' plasma, dihydroceramides, ceramides, sphingomyelins and glycosphingolipids that are downstream of Kdsr were not significantly different between Kdsr-depleted and control fish (supplemental Table 3B).

*Impaired proplatelet formation in MK from patients*

CFU-GEMM cultures differentiated from bone marrow HSC of the propositus showed hyperproliferation of myeloid cells ($p$=0·001, $t$-test) with a reduced myeloid/erythroid ratio compared to the controls (supplemental Figure 7). CFU-MK numbers

were comparable to those of the control, although individual MK colonies were denser for the propositus and liquid cultures showed an increased number of MK (supplemental Figure 8). MK in control cultures formed proplatelets, whilst MK derived from both the propositus and affected sister showed a strong reduction in proplatelet formation, despite similar levels of membrane budding and a higher number of CD41 and CD42 positive cells in propositus-derived cultures when compared with control MK (Figure 5A; supplemental Figure 8, 9, and 10). Patient-derived MK also showed extensive, abnormal formation of lamellipodia and reduced cell size ($p$=0·014, likelihood ratio test, Figures 5B and C).

*The abnormal morphological, functional, and biochemical features of the propositus' iMK can be rescued*

To corroborate the atypical phenotypes of MK derived from the HSC, we transduced iPSC from the propositus with lentiviral vectors containing the reference *KDSR* ORF ($K^{resc}$) or an inert control vector ($K^{ev}$), and reprogrammed these cells to iMK (supplemental Figure 11A). Analysis of the iMK RNA-seq results showed similar *KDSR* gene expression but the majority of sequencing reads in the rescued iMK carried the reference allele at Chr18:61018270 G>A (p.Arg154Trp, supplemental Figures 11B, C and D). These findings are consistent with correction of the genetic defect without significant overexpression, and resulted in increased proplatelet formation compared with control iMK four hours after seeding (Figures 6A, B and C; $p$=0·047, $t$-test). The observed iMK proplatelets were shorter and less branched than those observed following directed differentiation from stem cell cells, in keeping with published reports using this protocol.[17] Upon microscopic inspection the rescued iMK seemed larger than the non-rescued ones (which was confirmed to be significant by flow cytometry, supplemental Figure 11E) and the increased proplatelet formation resulted by 24 hours in little residual cytoplasm for the rescued versus the non-rescued iMK (Figure 6C). At the biochemical level the rescue resulted in a significant reduction of KDS levels ($p$=0·02, $t$-test) showing the effectiveness of the gene therapy approach in 'curing' the iMK from the propositus (Figure 6D). Similar to findings in plasma and in zebrafish, DHS levels did not differ between the iMK with and without functional *KDSR* transcripts, indicating that the postulated, compensatory mechanism is also present in iMK. We searched the iMK transcriptome landscape for possible differences in the levels of transcripts of other key enzymes that regulate sphingolipid synthesis and recycling (the enzymes examined are as shown in Figure 3A). This identified only *ASAH1* and *CERS6* transcripts to be down- and up- regulated respectively (posterior probabilities 0·610 and 0·774; log fold change -0·67 and +0·70, respectively). These two enzymes regulate the ceramide-sphingosine ratio (Figure 3A, supplemental Figure 12) and in keeping with these findings, the rescued iMK showed higher sphingosine and lower ceramide levels (Figure 6D).

**Discussion**

Pathogenic mutations in *KDSR* have recently been associated with a recessively inherited syndrome of moderate-to-severe skin pathology and thrombocytopenia.[8, 9] We have described two novel *KDSR* mutations causing thrombocytopenia in the propositus and his infant sister, expanding the phenotypic spectrum of this recently identified Mendelian disorder from severe skin pathology with no apparent hematological involvement to profound thrombocytopenia and moderate anemia with spontaneous improvement across the first decade, and almost imperceptible dermatological abnormalities. In the propositus bone marrow studies also showed the novel phenotype of severe juvenile myelofibrosis, however the sister was too young to allow confirmation of this phenotype. The biochemical sphingolipid signatures of the plasma and patient-derived iMK confirmed the predicted reduction in function with elevated levels of its substrate, KDS. This is as expected, from the combination of a variant encoding a premature stop codon and a hypomorphic allele involving a missense variant in the catalytic domain. Unexpectedly, downstream metabolites in the sphingolipid pathway including DHS, ceramide, and sphingosine-1-phosphate were not reduced in plasma, suggesting that *KDSR* hypofunction during *de novo* sphingolipid synthesis is compensated by an alternative pathway. One possible alternative pathway is the recycling of relatively abundant sphingomyelins, a pathway previously shown to contribute to production of downstream sphingolipids such as dihydroceramide, ceramide, and sphingosine, but considered to contribute little, if at all to DHS production under normal conditions.[21] Post-translational modifications to sphingolipid enzymes may also explain the metabolic

profile, and further work is required to explore this possibility. Importantly, the profile of increased ceramide and reduced sphingosine in propositus-derived iMK compared with rescued iMK, and the consistent and potentially explanatory transcriptional dysregulation of enzymes ASAH1 and CERS6, is at odds with the limited sphingolipid quantitation undertaken in previous studies which showed that ceramide levels were reduced in affected skin and that platelet surface exposure of ceramide was impaired in individuals with hypo-functional *KDSR* variants.[9]

Our observation that MK lacking functional KDSR are hyperproliferative is consistent with earlier reports,[9] but we expand on this characterisation by showing the *ex-vivo* generated patient MK to be smaller than controls and to be less effective in proplatelet formation. Proplatelets are pseudopodial projections of megakaryocyte cytoplasm, supported at their core by microtubular bundles that carry granules and other platelet cargo from the body of the megakaryocyte to the tip of the proplatelet.[22] Aberrant size and proplatelet formation were not only observed in MK obtained by differentiation of primary HSC obtained from the two patients, but are also present in iMK generated by forward programming of iPSC derived from the propositus' fibroblasts. All together we consider the ineffective platelet formation caused by the absence of KDSR to be the primary cause of the thrombocytopenia. Increased turn-over because of a reduced platelet lifespan seems to be a less likely explanation because the immature platelet fraction was not significantly raised in the two patients compared with healthy controls (data not shown). We hypothesize that impaired platelet formation may, in turn, be caused by cytoskeletal disorganisation and further experiments are required to explore this possibility. Pathogenic mutations in several other genes (e.g. *MYH9, ACTN1, FLNA, TUBB1, DIAPH1, TPM4*) encoding proteins with important functional roles in cytoskeletal reorganisation and actin polymerisation are causal of dominant forms of thrombocytopenia.[23] However these genetic disorders are characterised by enlarged platelets, and the mean volumes of the platelets of our patients are within the normal ranges for males and females, respectively.

The increased level of KDS in plasma was confirmed at the cellular level in iMK derived from the propositus. This increased level was normalised upon rescue of the propositus' iMK with a *KDSR* transcript carrying the reference allele. The correction of the biochemical defect was mirrored by a recovery of iMK size and improvement of their capacity to form proplatelets. In further support of the central importance of KDSR in thrombopoiesis we show that KDSR knockdown in a zebrafish model is associated with impaired thrombocyte formation. Similar approaches have identified multiple potential regulators of thrombopoiesis,[24] though in isolation zebrafish studies are limited by inherent differences in thrombopoiesis between mammals and fish, notably that zebrafish have nucleate thrombocytes rather than MK.

The marked, spontaneous improvement of the propositus' thrombocytopenia and anemia led to reversal of the decision to treat the condition by HSC transplantation. The mechanism of this improvement is unclear, given the presence of progressive myelofibrosis and in the absence of clinical features to suggest significant extramedullary hemopoiesis such as splenomegaly. Recent studies have shown spontaneous improvement in blood counts in other inherited juvenile bone marrow failure syndromes, most notably those associated with pathogenic variants in *SAMD9* or *SAMD9L*.[25] In these cases the improvement was attributed to the acquisition of corrective somatic mutations. Further longitudinal studies of individuals affected by pathogenic *KDSR* variants is essential to determine whether the clinical course described is representative, and whether a careful watch-and-wait approach rather than early intervention may be more appropriate in this genetically-defined subgroup of cases with inherited thrombocytopenia accompanied by bone marrow failure.

**Funding**

T.K.B is supported by the British Society of Haematology and NHS Blood and Transplant. K.F and C.V.G. are supported by the Fund for Scientific Research-Flanders (FWO Vlaanderen, Belgium; G.0B17.13N) and by the Research Council of the University of Leuven (BOF KU Leuven, Belgium; OT/14/098). C.V.G is holder of the Bayer and Norbert Heimburger (CSL Behring) Chairs. The structured illumination microscope was acquired through a CLME grant from Minister Lieten to the VIB BioImaging Core, Leuven. J.H is supported by the Fund for Scientific Research-Flanders (FWO Vlaanderen, Belgium) grant no.1S00816N. A.K and B.J are funded by the National Institute for Health Research (NIHR) Biomedical Research Centre (RG64245). M.F. is supported by the British Heart Foundation (BHF) Cambridge Centre of Excellence (RE/13/6/30180). The Ouwehand laboratory receives support from the BHF, Bristol-Myers Squibb, European Commission, MRC, NHS Blood and Transplant, Rosetrees Trust, the NIHR Biomedical Research Centre based at Cambridge University Hospitals NHS Foundation Trust, and the University of Cambridge.

**Acknowledgements**

The NIHR BioResource – Rare Disease Study is a multicentre whole-genome sequencing (WGS) study of approximately 13,000 patients. The genotype and phenotype data are being incorporated in the 100,000 Genomes Project. This study makes use of data generated by the NIHR BioResource and a full list of investigators who contributed to the generation of the data is available from https://bioresource.nihr.ac.uk/rare-diseases/consortia-lists/. Funding for the project was provided by the NIHR (grant number RG65966). The NIHR BioResource projects were approved by Research Ethics Committees in the UK and appropriate national ethics authorities in non-UK enrolment centres. The authors are also grateful to all the research participants who donated their samples for this study and to Professor Andrew Mumford (University of Bristol, Bristol, UK), Professor Michael Laffan (Imperial College London, London, UK), Dr Lining Guo (Metabolon Inc, Durham, NC), and Dr Sergio Rodriguez-Cuenca and Professor Antonio Vidal-Puig from the University of Cambridge (Cambridge, UK) for their input. The Tg(cd41:EGF)[11] line was a gift from Professor Leonard Zon (Hematology Division, Brigham and Women's Hospital, Boston, MA).

**Authorship contributions**

T.K.B analysed the results, performed the iPSC and iMK experiments, and wrote the manuscript. E.T and D.G performed statistical analyses and E.T edited the manuscript. C.T. performed stem cell differentiations. J.H. performed granule immunostainings and quantifications. M.D.R. performed zebrafish experiments. F.B assisted with cDNA library synthesis. L.G and D.S performed RNA-seq analysis. B.J performed mass spectrometry of sphingolipids. M.F and A.K analysed results and edited the paper. D.W provided sample logistics, QC and whole genome sequencing oversight. O.S analysed the sequencing results. C.G and K.G edited the paper. V.L and C.V.G are clinicians following up this pedigree. W.H.O leads the NIHR BioResource- Rare Diseases and co-wrote the paper. K.F. designed the study and analysis plan, and co-wrote the paper.

**Conflict of Interest Disclosures**

The authors have declared that no conflict of interest exists.

**References**


1. Kihara A, Igarashi Y. FVT-1 is a mammalian 3-ketodihydrosphingosine reductase with an active site that faces the cytosolic side of the endoplasmic reticulum membrane. J Biol Chem. 2004;279(47):49243-49250.
2. Chen L, Kostadima M, Martens JH, et al. Transcriptional diversity during lineage commitment of human blood progenitors. Science. 2014;345(6204):1251033.
3. Battle A, Brown CD, Engelhardt BE, Montgomery SB. Genetic effects on gene expression across human tissues. Nature. 2017;550(7675):204-213.
4. Hannun YA, Luberto C, Argraves KM. Enzymes of sphingolipid metabolism: from modular to integrative signaling. Biochemistry. 2001;40(16):4893-4903.
5. Munzer P, Schmid E, Walker B, et al. Sphingosine kinase 1 (Sphk1) negatively regulates platelet activation and thrombus formation. Am J Physiol Cell Physiol. 2014;307(10):C920-927.
6. Munzer P, Borst O, Walker B, et al. Acid sphingomyelinase regulates platelet cell membrane scrambling, secretion, and thrombus formation. Arterioscler Thromb Vasc Biol. 2014;34(1):61-71.
7. Tani M, Sano T, Ito M, Igarashi Y. Mechanisms of sphingosine and sphingosine 1-phosphate generation in human platelets. J Lipid Res. 2005;46(11):2458-2467.
8. Boyden LM, Vincent NG, Zhou J, et al. Mutations in KDSR Cause Recessive Progressive Symmetric Erythrokeratoderma. Am J Hum Genet. 2017;100(6):978-984.
9. Takeichi T, Torrelo A, Lee JYW, et al. Biallelic mutations in KDSR disrupt ceramide synthesis and result in a spectrum of keratinization disorders associated with thrombocytopenia. J Invest Dermatol. 2017;137(11):2344-2353.
10. Freson K, De Vos R, Wittevrongel C, et al. The TUBB1 Q43P functional polymorphism reduces the risk of cardiovascular disease in men by modulating platelet function and structure. Blood. 2005;106(7):2356-2362.
11. Long T, Hicks M, Yu HC, et al. Whole-genome sequencing identifies common-to-rare variants associated with human blood metabolites. Nat Genet. 2017;49(4):568-578.
12. Koulman A, Woffendin G, Narayana VK, Welchman H, Crone C, Volmer DA. High-resolution extracted ion chromatography, a new tool for metabolomics and lipidomics using a second-generation orbitrap mass spectrometer. Rapid Commun Mass Spectrom. 2009;23(10):1411-1418.
13. Lu L, Koulman A, Petry CJ, et al. An Unbiased Lipidomics Approach Identifies Early Second Trimester Lipids Predictive of Maternal Glycemic Traits and Gestational Diabetes Mellitus. Diabetes Care. 2016;39(12):2232-2239.
14. Lin HF, Traver D, Zhu H, et al. Analysis of thrombocyte development in CD41-GFP transgenic zebrafish. Blood. 2005;106(12):3803-3810.
15. Louwette S, Labarque V, Wittevrongel C, et al. Regulator of G-protein signaling 18 controls megakaryopoiesis and the cilia-mediated vertebrate mechanosensory system. FASEB J. 2012;26(5):2125-2136.
16. Louwette S, Regal L, Wittevrongel C, et al. NPC1 defect results in abnormal platelet formation and function: studies in Niemann-Pick disease type C1 patients and zebrafish. Hum Mol Genet. 2013;22(1):61-73.
17. Moreau T, Evans AL, Vasquez L, et al. Large-scale production of megakaryocytes from human pluripotent stem cells by chemically defined forward programming. Nat Commun. 2016;7:11208.
18. Lek M, Karczewski KJ, Minikel EV, et al. Analysis of protein-coding genetic variation in 60,706 humans. Nature. 2016;536(7616):285-291.
19. Kircher M, Witten DM, Jain P, O'Roak BJ, Cooper GM, Shendure J. A general framework for estimating the relative pathogenicity of human genetic variants. Nat Genet. 2014;46(3):310-315.
20. Gupta SD, Gable K, Han G, et al. Tsc10p and FVT1: topologically distinct short-chain reductases required for long-chain base synthesis in yeast and mammals. J Lipid Res. 2009;50(8):1630-1640.
21. Kitatani K, Idkowiak-Baldys J, Hannun YA. The sphingolipid salvage pathway in ceramide metabolism and signaling. Cellular Signal. 2008;20(6):1010-1018.
22. Italiano JE, Jr., Lecine P, Shivdasani RA, Hartwig JH. Blood platelets are assembled principally at the ends of proplatelet processes produced by differentiated megakaryocytes. J Cell Biol. 1999;147(6):1299-1312.
23. Lentaigne C, Freson K, Laffan MA, Turro E, Ouwehand WH. Inherited platelet disorders: toward DNA-based diagnosis. Blood. 2016;127(23):2814-2823.
24. Bielczyk-Maczynska E, Serbanovic-Canic J, Ferreira L, et al. A loss of function screen of identified genome-wide association study Loci reveals new genes controlling hematopoiesis. PLoS Genet. 2014;10(7):e1004450.
25. Bluteau O, Sebert M, Leblanc T, et al. A landscape of germ line mutations in a cohort of inherited bone marrow failure patients. Blood. 2018;131(7):717-732.

**Figure 1. Reported *KDSR* variant genotypes and phenotypes in the context of KDSR structure and function**

Protein and cDNA schematic adapted from Gupta *et al*[20] demonstrating location of known pathogenic *KDSR* variants with documented phenotypes in skin only (black), skin and platelets (red) and the novel variants reported in this manuscript in bold and underlined. Variants are linked by brackets where present in compound heterozygosity in an individual. Key structural elements of KDSR are illustrated: transmembrane anchors (blue, purple), the Rossman folds (red), and a highly conserved domain containing three putative catalytic sites (yellow). The novel p.Arg154Trp variant is within the catalytic domain.

**Figure 2. Clinical characteristics associated with loss-of-function *KDSR* variants**

(A) Pedigree and variants identified in *KDSR*. '+' denotes the major allele. The propositus and affected sibling,
but not the healthy sibling, carry the missense variant 18:61018270 G>A (p.Arg154Trp) and the nonsense variant 18:61006104 G>A (p.Arg236*). Co-segregation analysis demonstrated that the father carries the former and the mother the latter variant. (B) Serial blood counts are shown for the two affected siblings and a single value for the healthy brother. Fluctuating anemia and thrombocytopenia was observed, without evidence of neutropenia. (C) Bone marrow biopsy. Left: Numerous dysplastic megakaryocytes made visible with LAT staining are present. Right: Marrow fibrosis with strong stromal reticulin staining. Magnification x40. Further images can be found in the supplemental materials. (D) The affected sibling was born during the course of this study and presented at birth with thrombocytopenia and mild ichthyosis in her left axilla. The skin symptoms improved spontaneously over the first month. (E) Platelets were examined by electron microscopy for an unrelated healthy control, the propositus, and the affected sibling. There were no marked morphological differences. Arrowed magnifications show δ-granules. Magnification 12,000x.

**Figure 3. Metabolic profiling shows that the *KDSR* variants are associated with loss-of-function and downstream sphingolipid pathway compensation**

(A) Simplified sphingolipid pathway highlighting the role of the KDSR enzyme in *de novo* synthesis (black arrows) and the generation of sphingolipid intermediates from the recycling of complex sphingolipids and sphingomyelins (green arrows). (B) Mass spectrometry using the Metabolon platform shows the major chromatographic peak of 3-keto-dihydrosphingosine (KDS) in the plasma of the propositus, but not of the unaffected pedigree members (shown) or the controls (not shown). (C) KDSR hypofunction was confirmed in the propositus and affected sister using a second mass spectrometry platform for targeted sphingolipid profiling. The chromatogram shows that KDS was detected in the plasma from the propositus and his affected sister but not in the plasma from the healthy brother, parents (shown), and two controls (not shown).

**Figure 4. *Kdsr* morpholino knockdown is associated with reduced thrombopoiesis in zebrafish**

(A) Tg(cd41:EGF) embryos were injected with a kdsr ATG-MO (1000 µM) or with buffer (control). Embryos were lysed 72 hpf and used for immunoblotting. GFP and Kdsr proteins were reduced in the kdsr knockdown condition. Equal amounts (50 µg) were loaded (5 randomly selected embryos for each of the 4 conditions). Staining of Gapdh was used as loading control. (B) Quantification of immunoblot after normalization for Gapdh. Mean values are plotted and error bars show the standard deviation, analysed by one-way ANOVA. (C) Quantification by flow cytometry of the number of GFP-labelled thrombocytes in Tg(cd41:EGFP) *Danio rerio* embryos at 72 hpf for kdsr-MO (800 or 1000 µM) or buffer (control) injected fish. Values are means and standard deviations (SD) as quantified for 10 randomly selected embryos for each condition, performed in triplicate. Results were analyzed by one-way ANOVA. (D) Greyscale stereo-microscope images (20x original magnification) in the tail region at 72 hpf showed a reduced number of GFP-labelled thrombocytes (in white). (E) KDS levels in lysates from 72 hpf embryos (20/condition) for kdsr-MO (800 µM) or buffer (control) injected fish. KDS was detected in the lysates from the MO-injected embryos but not in the control-injected embryos.

**Figure 5. *KDSR* variants are associated with reduced proplatelet formation by megakaryocytes (MK)**

(A) Quantification of proplatelet formation by MK at day 11 of differentiation. On the left are the results of differentiation of bone marrow-derived hematopoietic stem cells (HSC) from the propositus and control. On the right are the results of differentiation of HSC obtained from the blood of the propositus, his affected sibling and a second control. All MK with proplatelets and membrane budding were counted as positive. Values plotted are means and standard deviations (SD) as quantified on 20 images. Results were analyzed by the unpaired, two-tailed t-test. (B) MK at day 11 derived from bone marrow HSC from the propositus and a control. MK are stained for the cytoskeletal marker F-actin (red) and lysosome and δ-granule marker CD63 (green). MK from the propositus and affected sibling have irregular cytoskeletal structures with

lamellipodia (arrows). Further images can be found in supplemental Figure 10. (C) MK area was quantified by automated analysis. Modelling was performed using a linear mixed effects model and associated *p*-values were computed by a likelihood ratio test. MK from affected cases were smaller compared to unrelated controls ($p$=0·01473).

**Figure 6. *KDSR* reference allele expression rescues ineffective proplatelet formation**

Proplatelet formation by iMK. 100% of live MK plated for the proplatelet assay were CD41 positive and 75% were dual positive for CD41 and CD42 by flow cytometry (supplemental Figure 11A). Cytoskeletal marker α-tubulin was stained with antibodies in green and nuclei were stained with DAPI in blue. Proplatelet formation was counted manually. Values shown were analyzed using the paired, two-tailed Student's *t*-test, using $p$<0·05 for significance and are plotted as means and standard deviations. (A) The number of proplatelets formed at 4 hours per proplatelet-forming MK (PPFMK) by the rescued and non-rescued iMK. The differences were significant at 4 hours ($p$=0·047) but not anymore at 24 hours ($p$=0·20). (B) The number of PPFMK at 4 hours did not differ significantly between the two groups (7·1% vs 42·4% , $p$=0·10), but at 24 hours the rescued showed less PPFMK ($p$=0·03). (C) Representative images from the proplatelet formation assay at 4 and 24 hours. Proplatelets are indicated by white arrows. Top left and right panel: Results at 4 hours for rescued iMK show increased proplatelet formation. White scale bars indicate 10µm. Bottom left and right panel: Results at 24 hours show little proplatelet formation for the rescued iMK, and residual cells are either fragmented into platelet-like particles, or consist of bare nuclei. (D) Metabolon mass spectrometry results for non-rescued and rescued iMK. The ion counts for KDS detection differed significantly between the non-rescued and non-rescued iMK ($p$=0·02). The DHS level did not differ between the groups of samples but the levels of sphingosine and ceramide were lower and higher in the non-rescued versus rescued iMK, respectively.

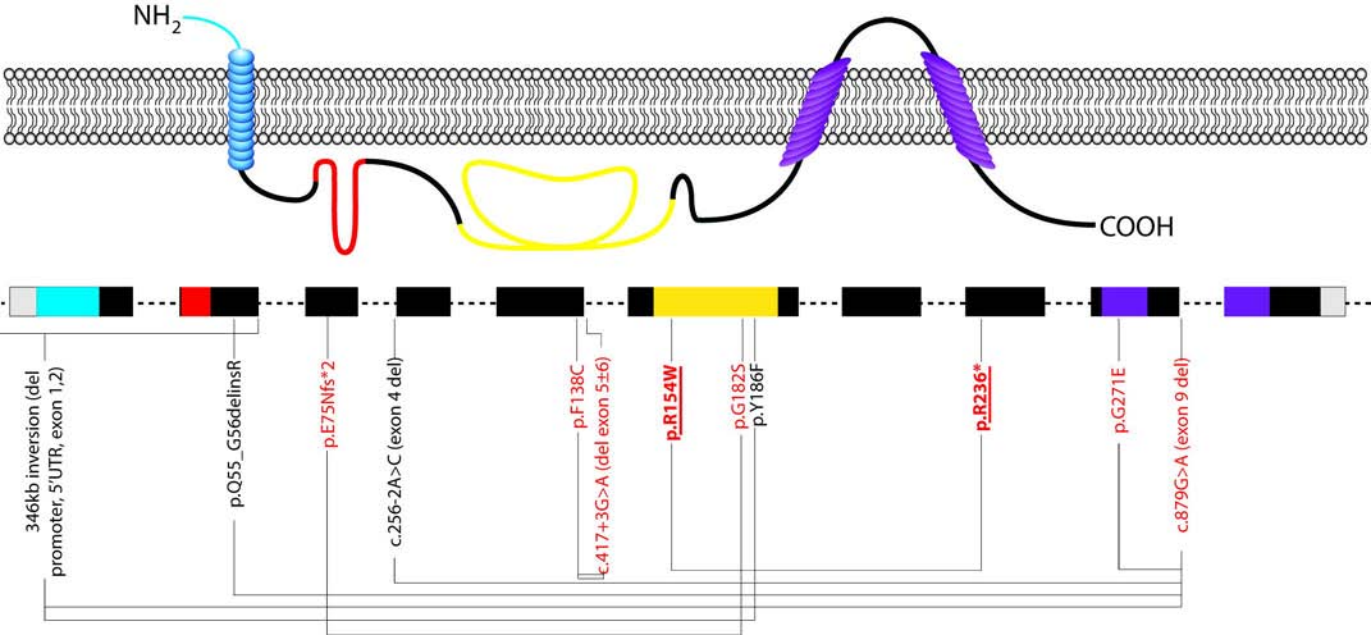
NH2
COOH
346kb inversion (del promoter, 5'UTR, exon 1,2)
p.Q55_G56delinsR
p.E75Nfs*2
c.256-2A>C (exon 4 del)
p.F138C
c.417+3G>A (del exon 5±6)
p.R154W
p.G182S
p.Y186F
p.R236*
p.G271E
c.879G>A (exon 9 del)

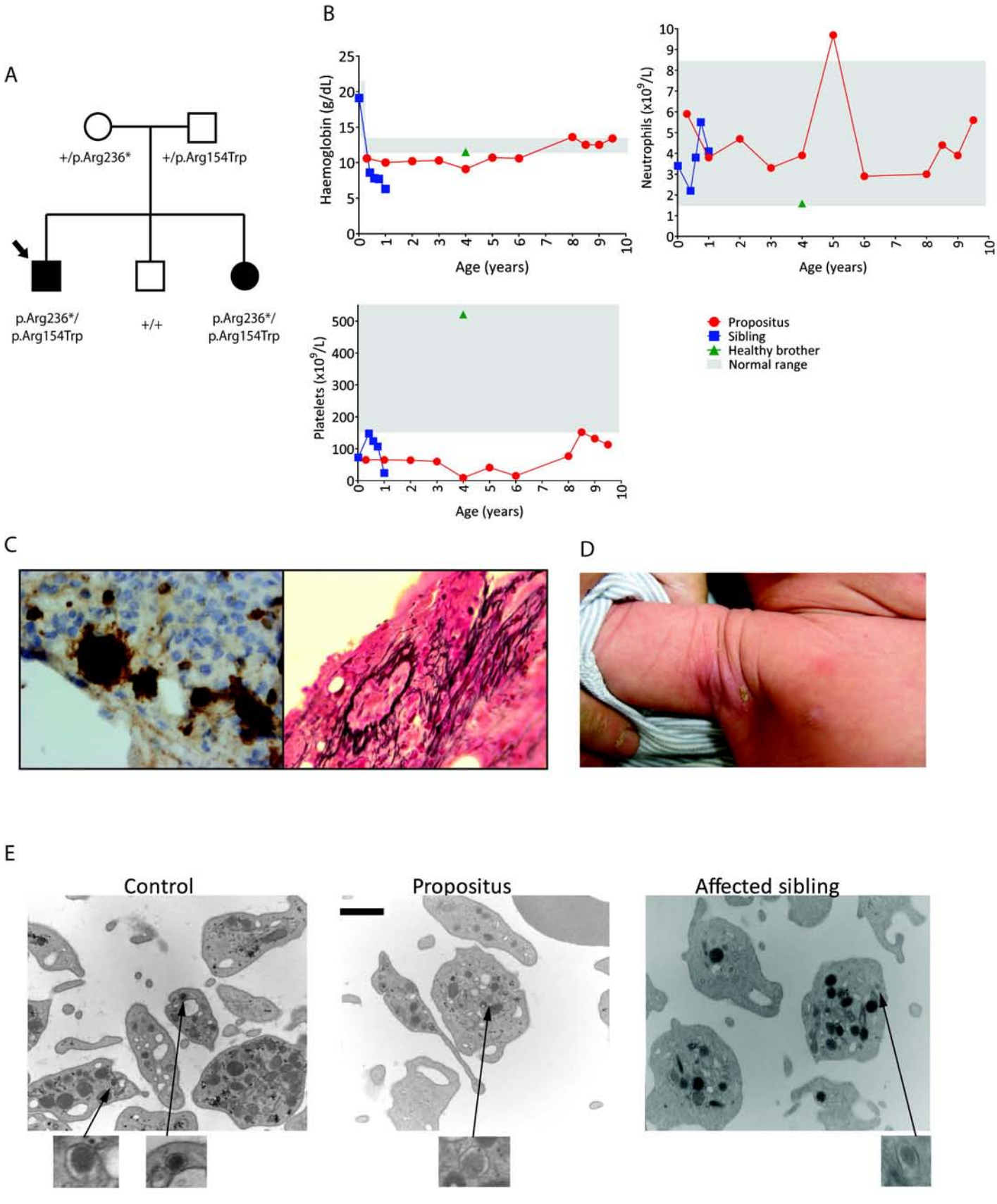
A
+/p.Arg236*
+/p.Arg154Trp
p.Arg236*/
p.Arg154Trp
+/+
p.Arg236*/
p.Arg154Trp
B
Haemoglobin (g/dL)
Age (years)
Neutrophils (x10^9/L)
Age (years)
Platelets (x10^9/L)
Age (years)
Propositus
Sibling
Healthy brother
Normal range
C
D
E
Control
Propositus
Affected sibling

A

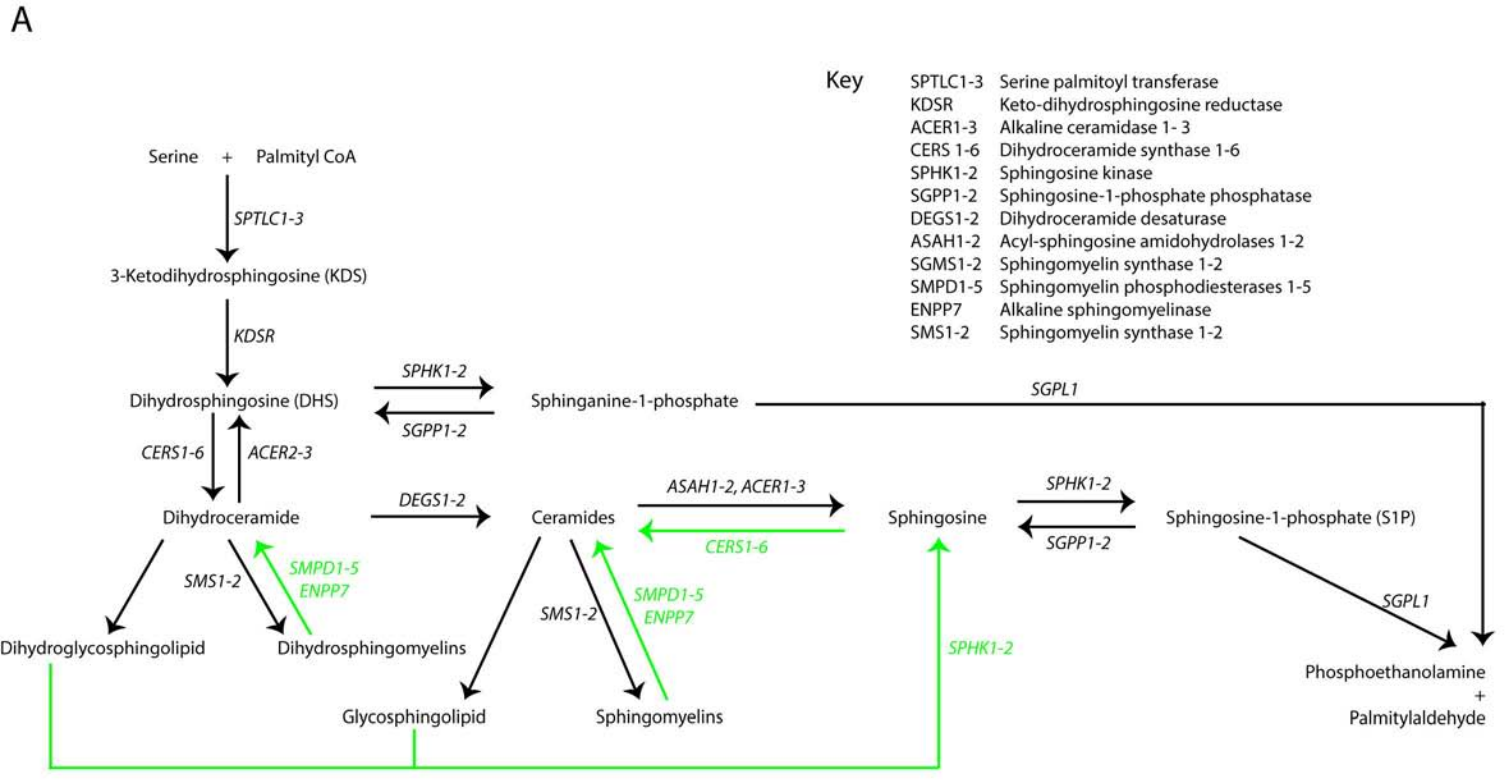
Key
SPTLC1-3 Serine palmitoyl transferase
KDSR Keto-dihydrosphingosine reductase
ACER1-3 Alkaline ceramidase 1- 3
CERS 1-6 Dihydroceramide synthase 1-6
SPHK1-2 Sphingosine kinase
SGPP1-2 Sphingosine-1-phosphate phosphatase
DEGS1-2 Dihydroceramide desaturase
ASAH1-2 Acyl-sphingosine amidohydrolases 1-2
SGMS1-2 Sphingomyelin synthase 1-2
SMPD1-5 Sphingomyelin phosphodiesterases 1-5
ENPP7 Alkaline sphingomyelinase
SMS1-2 Sphingomyelin synthase 1-2
Serine + Palmityl CoA
SPTLC1-3
3-Ketodihydrosphingosine (KDS)
KDSR
Dihydrosphingosine (DHS)
SPHK1-2
SGPP1-2
Sphinganine-1-phosphate
SGPL1
CERS1-6
ACER2-3
Dihydroceramide
DEGS1-2
Ceramides
ASAH1-2, ACER1-3
CERS1-6
Sphingosine
SPHK1-2
SGPP1-2
Sphingosine-1-phosphate (S1P)
SMS1-2
SMPD1-5
ENPP7
SMS1-2
SMPD1-5
ENPP7
SGPL1
SPHK1-2
Dihydroglycosphingolipid
Dihydrosphingomyelins
Glycosphingolipid
Sphingomyelins
Phosphoethanolamine
+
Palmitylaldehyde

B

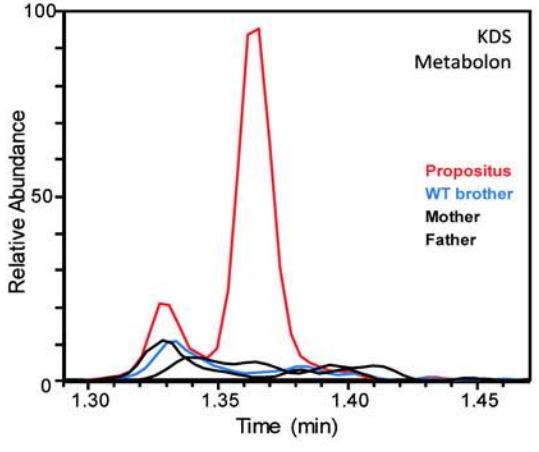
KDS
Metabolon
Propositus
WT brother
Mother
Father
Relative Abundance
100
50
0
1.30
1.35
1.40
1.45
Time (min)

C

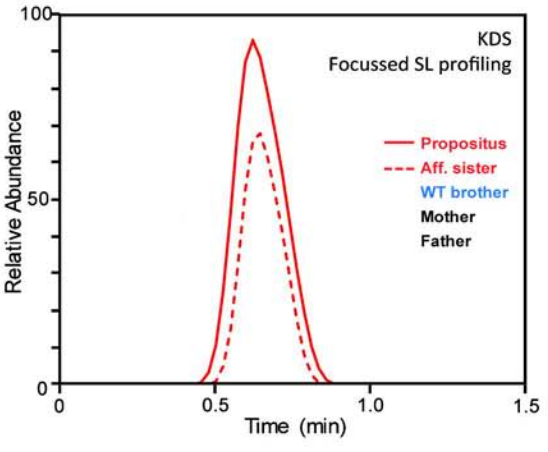
KDS
Focussed SL profiling
Propositus
Aff. sister
WT brother
Mother
Father
Relative Abundance
100
50
0
0
0.5
1.0
1.5
Time (min)

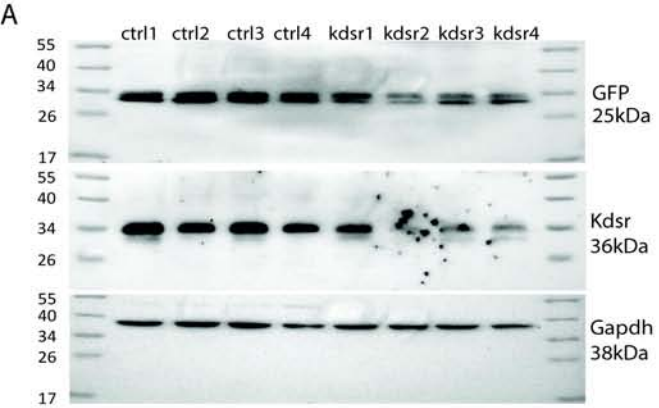
A
ctrl1 ctrl2 ctrl3 ctrl4 kdsr1 kdsr2 kdsr3 kdsr4
55
40
34
26
17
GFP
25kDa
Kdsr
36kDa
Gapdh
38kDa

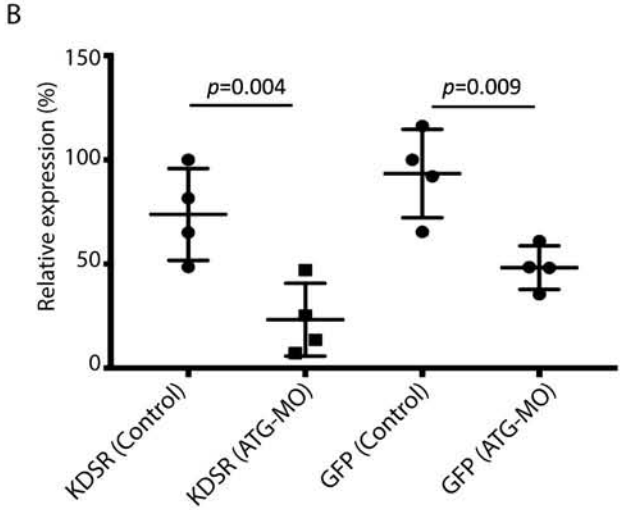
B
Relative expression (%)
150
100
50
0
p=0.004
p=0.009
KDSR (Control)
KDSR (ATG-MO)
GFP (Control)
GFP (ATG-MO)

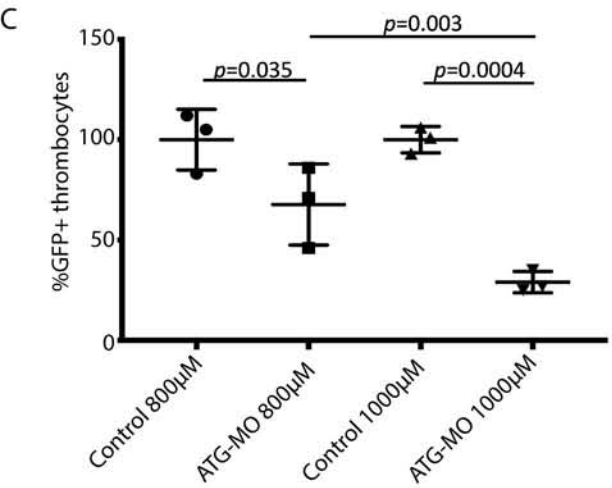
C
%GFP+ thrombocytes
150
100
50
0
p=0.003
p=0.035
p=0.0004
Control 800µM
ATG-MO 800µM
Control 1000µM
ATG-MO 1000µM

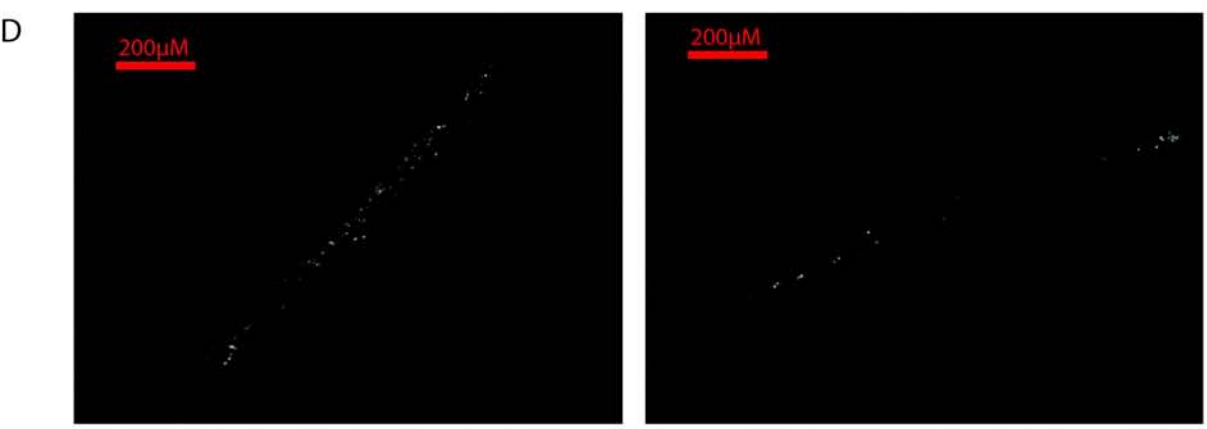
D
200µM
200µM

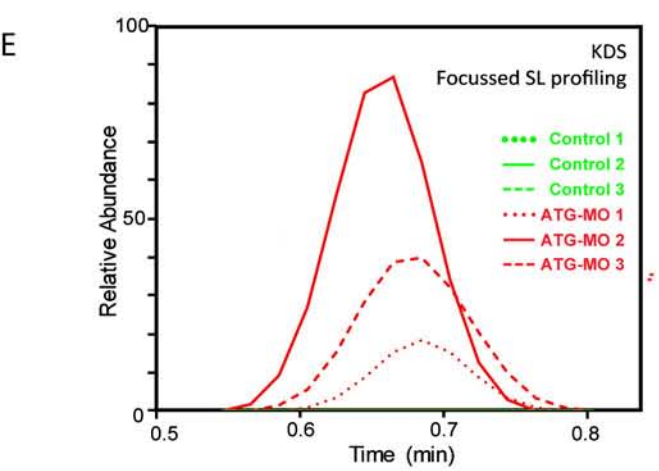
E
100
50
0
Relative Abundance
0.5
0.6
0.7
0.8
Time (min)
KDS
Focussed SL profiling
Control 1
Control 2
Control 3
ATG-MO 1
ATG-MO 2
ATG-MO 3

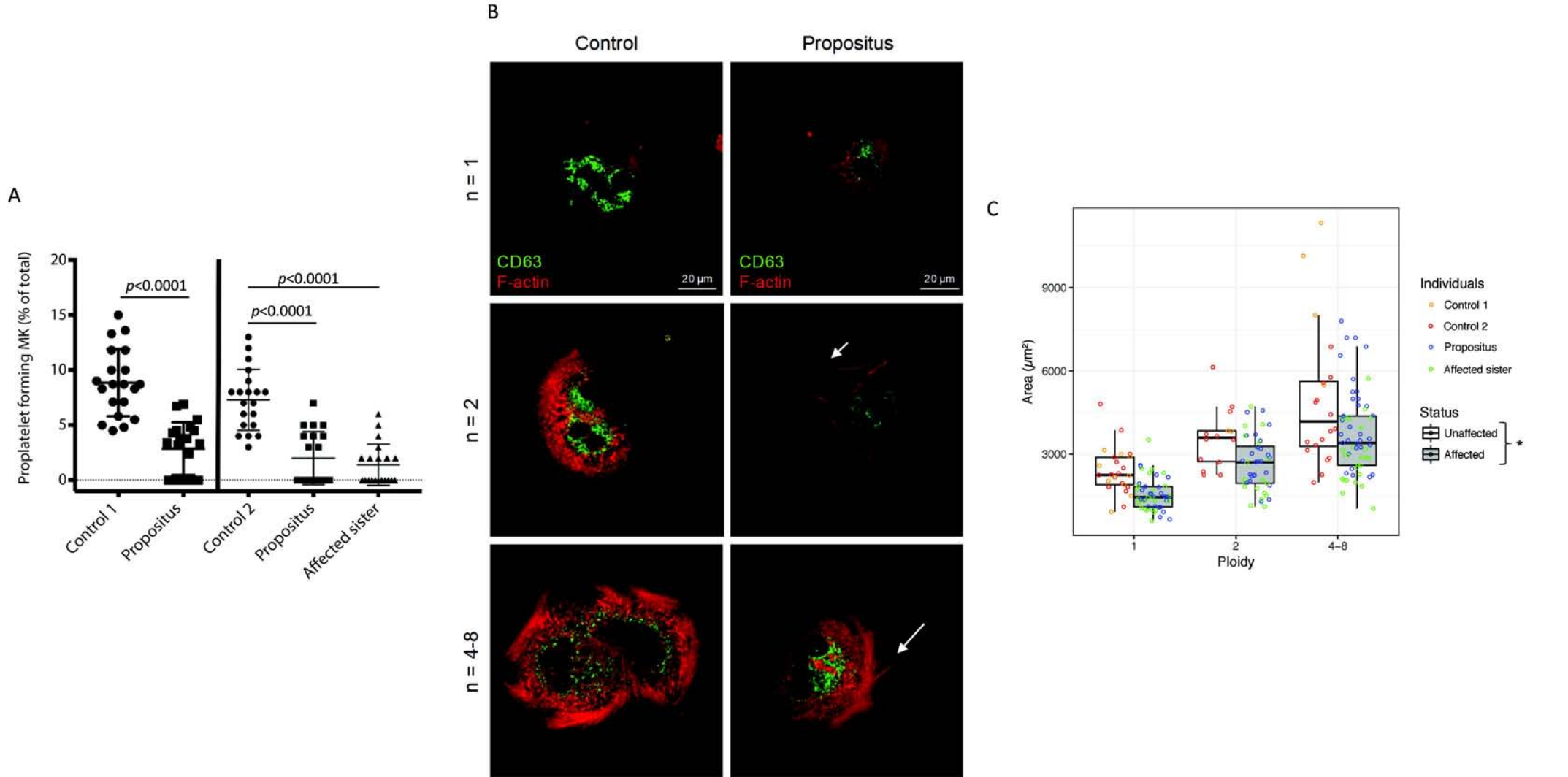
A
Proplatelet forming MK (% of total)
20
15
10
5
0
p<0.0001
p<0.0001
p<0.0001
Control 1
Propositus
Control 2
Propositus
Affected sister
B
Control
Propositus
n = 1
n = 2
n = 4-8
CD63
F-actin
20 µm
C
Area (µm²)
9000
6000
3000
1
2
4–8
Ploidy
Individuals
Control 1
Control 2
Propositus
Affected sister
Status
Unaffected
Affected
*

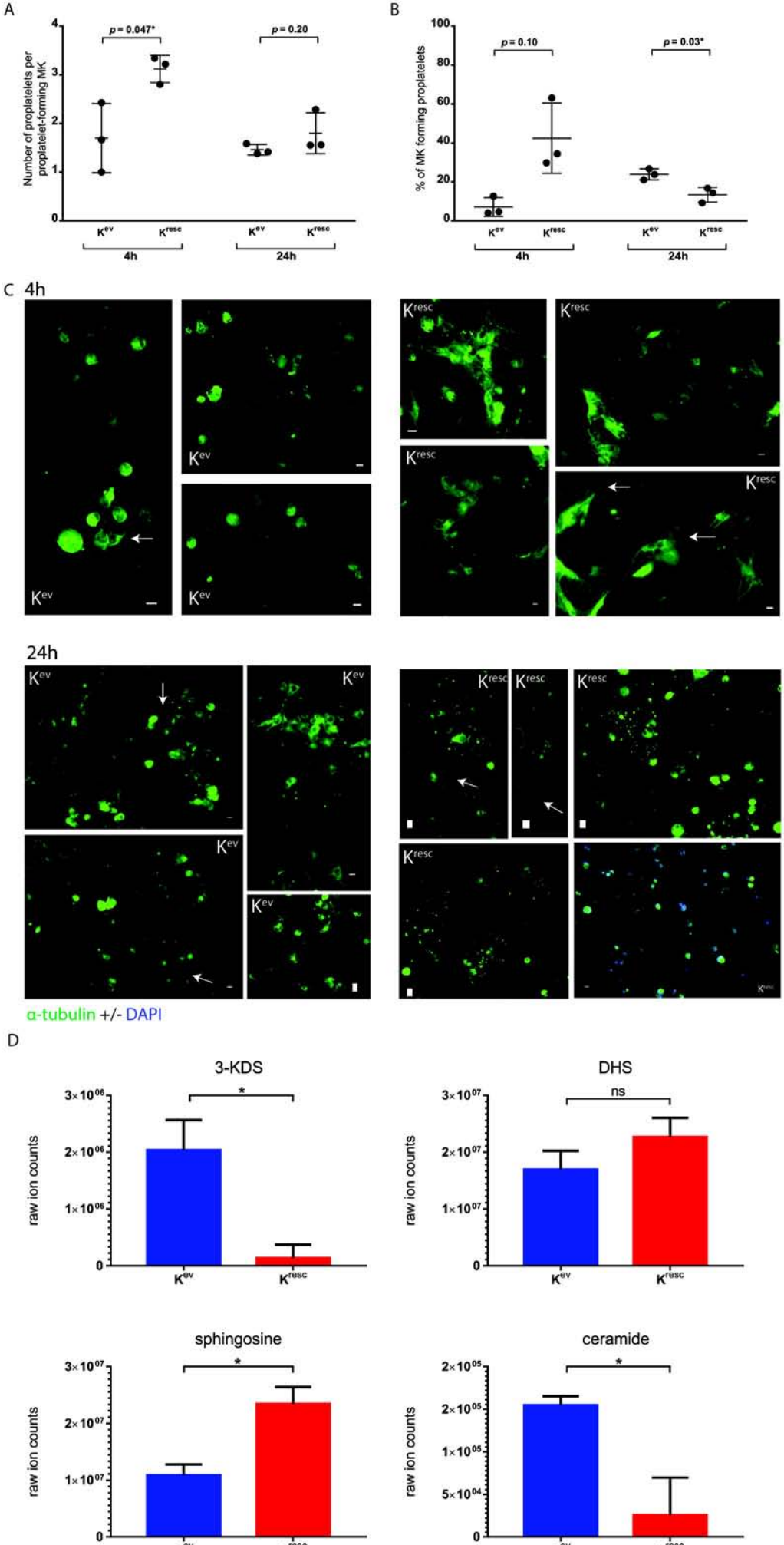
A
Number of proplatelets per proplatelet-forming MK
p = 0.047*
p = 0.20
K^ev
K^resc
4h
24h
B
% of MK forming proplatelets
p = 0.10
p = 0.03*
C 4h
24h
α-tubulin +/- DAPI
D
3-KDS
DHS
sphingosine
ceramide
raw ion counts
*
ns

# Supplemental Materials

## Supplemental Methods

*Recruitment and sequencing*

Genetic variants were identified from whole genome sequencing (WGS) data using Isaac (Illumina Inc.) or as described previously for whole exome sequencing.[1] Clinical and laboratory phenotypes were recorded in raw form and as Human Phenotype Ontology (HPO) terms along with pedigree data.[1] The propositus' genetic and phenotypic data were analyzed as part of a dataset of from 9,472 study participants that have undergone genetic analysis, which includes 1,472 cases with unexplained BPDs.

*Platelet imaging*

Platelet imaging was performed using a structured illumination microscope (SIM, Elyra S.1, Zeiss, Heidelberg, DE). Images were analyzed with ZEN Black (Carl Zeiss Inc., Oberkochen, DE) and ImageJ software (National Institutes of Health (NIH), Bethesda, MD).[2] Raw 3D SIM images were processed to super-resolution SIM using ZEN Black software, followed by maximum intensity projection as previously described.[3]

*Metabolic profiling*

In the targeted sphingolipid profiling protocol, for the identification of KDS we used a Thermo Scientific Q-Exactive Orbitrap (ThermoFisher Scientific, Hemel Hempstead, UK) set up to fragment the 300.3 ion (±2 m/z) using a relative collision energy of 30. The KDS standard used was purchased from Matreya LLC (Cat. no. 1876, State College, PA). All samples were snap frozen in dry ice and stored at -80$^0$C until analysed. Zebrafish lysates for sphingolipid profiling were prepared as for immunoblot analysis, using 20 embryos per condition, in triplicate, isolated at 72 hours post fertilisation [hpf].[4]

*Stem cell differentiation assays*

$CD34^+$ hematopoietic stem cells (HSC) isolated from bone marrow aspirates from the propositus (at 5 years of age) and an unrelated control, and from peripheral blood from the propositus (at 8·5 years of age), his affected sister (at 5 months of age) and an unrelated control were stored in liquid nitrogen. The recovered (differentiation day 0) CD34+ HSCs were cultured in StemSpan SFEM medium with StemSpan CC100 ensuring strong expansion of HSC for 3 days (Stem Cell Technologies, Vancouver, CA).

The expanded bone marrow derived HSC were used to perform colony assays for MK (CFU-MK) and granulocytes, erythrocytes, monocytes, and MK (GEMM; CFU-GEMM) as described previously.[4, 5] These were performed in quintuple for MegaCult-C 04973 (MK) and triplicate for MethoCult 04964 (GEMM, StemCell Technologies, Vancouver, CA). MK (after Giemsa staining) and GEMM (without staining) colonies were counted by two independent operators using a Zeiss Axiovert 200M microscope (Carl Zeiss Inc.) or light microscope (Leica DM RBE, Wetzlar, DE), respectively. Colonies from GEMM plates were further analysed by flow cytometry using FITC-labelled mouse antibodies against glycophorin A (CD235a; BD Biosciences, San Jose, CA) and PE-labelled mouse antibodies against CD45 (Clone T29/33; Dako, Glostrup, DK).

Liquid MK cultures were derived from bone marrow- and peripheral blood- derived HSC at day 3 of differentiation by incubation with 50ng/ml thrombopoietin (TPO), 25ng/ml stem cell factor, and 10ng/ml

interleukin 1β (Peprotech, Rocky Hill, NJ,). MK were analysed by flow cytometry on total differentiation day 7 with FITC-labelled antibodies against CD41 and CD42 (BD Biosciences) and on total differentiation day 11 for proplatelet formation and immunostaining of cytoskeletal proteins F-actin, phalloidin-rhodamine (Sigma, St Louis, MO), and anti-tubulin (ThermoFisher Scientific), and δ-granule and lysosome marker CD63 (Santa Cruz, Dallas, TX).[5, 6] For immunostaining MK were seeded for 4 hours on fibrinogen-coated coverslips and stained cells were photographed at 63x magnification with a confocal microscope (AxioObserver.Z1, Zeiss, Heidelberg, DE). MK cell size was determined by F-actin staining and images were analyzed with ImageJ software (NIH[2]). Three random control images were used to optimize parameters and MK were excluded if the ploidy was unclear following F-actin staining, as described.[7]

*Statistical analysis of MK size following immunostaining*

Using the lmer function from the R package lme4 a linear mixed effects model was fitted to the log of MK cell size:

$$y_{ijkl} = \alpha + \beta p_{ijk} + \gamma s_i + \xi f_j + \delta p_{ijk} s_i + \eta_i + \epsilon_{ijkl}$$

$$\eta_i \sim N(0, \sigma_\eta^2)$$

$$\epsilon_{ijkl} \sim N(0, \sigma_\epsilon^2)$$

where $y_{ijkl}$ corresponds to the *k*th observation for individual $i \in \{1,2,3,4\}$ obtained as part of experiment $j \in \{1,2\}$. The covariate $p_{ijk}$ is equal to 0, 1 or 2 depending on whether the ploidy was 1, 2 or between 4 and 8, respectively. The covariate $s_i$ equals 1 if individual *i* is a case and 0 otherwise. The covariate $f_j$ equals 1 if *j*=2 and 0 if *j*=1. The interaction term $\delta$ captures the difference in the ploidy-dependent slope between cases and controls. Inter-individual variation is modelled with normally distributed random effects ($\eta_i$).

The regression coefficients $\hat{\alpha}, \hat{\beta}, \hat{\gamma}, \hat{\xi}, \hat{\delta}$ were estimated by maximum likelihood and associated *p*-values were computed by a likelihood ratio test and were as follows:

MK cell size:

$\hat{\alpha} = 7.78075$

$\hat{\beta} = 0.35496$

$\hat{\gamma} = -0.42443$ $\quad p = 0.01473$

$\hat{\xi} = -0.05632$

$\hat{\delta} = 0.07197$ $\quad p = 0.2641$

*iPSC derivation*

iPSC were prepared by the Cambridge Biomedical Research Centre iPSC core laboratory from fibroblasts isolated from a 2mm skin biopsy of the propositus' upper arm. Fibroblasts were reprogrammed following the protocol of Yamanaka and colleagues[8, 9] by overexpression of transcription factors OCT4, SOX2, KLF4, and c-MYC using the CytoTune™-iPS 2·0 Sendai Reprogramming Kit (Invitrogen) followed by culture on mouse embryonic fibroblast feeder cells in chemically defined media. Following establishment of iPSC colonies, approximately one month after reprogramming, clones were picked, passaged to feeder-free conditions, and validated. iPSC were cultured feeder- and antibiotic- free in Essential 8 medium (ThermoFisher Scientific).

*Lentiviral particle production, transduction and selection*

Replication-deficient lentiviral vector particles were produced by transient co-transfection of HEK 293T cells with the rescue or empty vector and a 2nd generation packaging system consisting of psPAX2 and pCMV-VSV-

G (Addgene #12260, #8454). Viral particles were concentrated by the LentiX-concentrator system (Clontech). Transduction was performed in iPSC at MOI 2, in the presence of protamine sulphate 10μg/ml (Sigma) and was followed by plate centrifugation at 2500 rpm for 45 minutes at 37$^0$C. Cells carrying the rescue or empty vector were selected after 72 hours using 0·1μg/ml puromycin (Sigma).

*Forward programming to MK (iMK)*

Passage to single iPSC was obtained using TrypLE (ThermoFisher Scientific) followed by culture in Essential 8 media containing 10μM ROCK inhibitor (Sigma) for 24 hours prior to lentiviral transduction with *FLI1, GATA1,* and *TAL1* using a protocol for generating MK described by Moreau *et al.*[10] The MK obtained by this protocol (named iMK hereafter) were defined at day 20 post-transduction by absence of staining with 1μg/ml DAPI (Sigma; at this concentration live iMK are impermeant to DAPI) and dual staining with anti-CD41a-APC and anti-CD42b-PE (1:100, cat. 559777 and 1:1000, cat. 555473, respectively, BD Biosciences) on the Beckman Coulter Gallios Cytometer. Cytometry results were analysed using Kaluza Analysis v.1.5a (Beckman Coulter).

*Proplatelet assay*

iMK were placed at a concentration of 0·5x10$^6$/ml in CellGro medium (CellGenix) for seeding on sterile glass coverslips coated with 200μg/ml fibrinogen (Sigma**)** in phosphate-buffered saline (PBS). Cells were fixed in 1% paraformaldehyde at 4 hours or 24 hours after seeding. Cells were quenched with 50μM ammonium chloride and permeabilized with 0·1% saponin, 0·2% gelatin, and 0·02% azide (Sigma) in PBS. Staining was performed with antibody against α-tubulin (1:250, cat.T5168, Sigma), 1μg/ml DAPI (Sigma), and goat anti-mouse Alexa Fluor 488 antibody (1:1000, cat. A21121, ThermoFisher Scientific). Cells were examined within 48 hours using a Leica DMi8 fluorescent microscope and images were analysed using FIJI software.[2] Five to ten representative fields were examined to ensure at least 100 iMK were observed for each experimental condition. Proplatelets were defined as clear projections from the main cell body with approximately parallel sides to the shaft. Results were compared using the paired, two-tailed Student's *t*-test.

*RNA sequencing*

1 x 10$^5$ iMK were stored in 500 μl Trizol reagent (ThermoFisher Scientific) at -80$^0$C. RNA was recovered for sequencing (RNA-seq) with the Direct-zol RNA MiniPrep kit (Zymo). RNA was quantified using the Qubit RNA HS Assay kit (ThermoFisher Scientific) and its quality was confirmed using the Agilent RNA 6000 Pico kit on the Agilent 2100 Bioanalyzer. cDNA libraries were prepared using the KAPA Stranded RNA-Seq Kit with Riboerase (Roche) and Agencourt AMPure XP beads (Beckman Coulter) for purification. Libraries were quantified by RT-qPCR with the KAPA Library Quantification Kit (Roche). Libraries were sequenced at the Cancer Research UK Cambridge Institute Genomics Core) on a HiSeq4000 (Illumina Inc.) using 150bp read length paired-end sequencing. Sequences were aligned with STAR[11] and read counts were obtained using featureCounts[12] with respect to Ensembl v.70 of reference genome build GRCh37. Expression of transcripts and genes was quantified using MMSEQ and differential expression was assessed using MMDIFF[13, 14]. The prior probability of differential expression was set to 0·1 and a posterior probability >0·5 was used to declare a transcript being differentially expressed.

**Supplemental Table 1: Clinical data**

**(A)** Serial blood results for propositus and pedigree members. Abnormal results are shown in bold. Spontaneous improvements in both platelet count and hemoglobin level were observed in the propositus, though the improvement in platelet count was not sustained. The affected sibling's platelet count and haemoglobin values have been decreasing since birth.

| | **WBC ($x10^9$/L)** | **Neutrophils ($x10^9$/L)** | **Erythrocytes ($x10^6$/L)** | **Reticulocytes ($x10^9$/L)** | **Immature reticulocyte fraction (%)** | **Hemoglobin (g/dL)** | **Platelets ($x10^9$/L)** |
|---|---|---|---|---|---|---|---|
| ***Control values Neonates (<6 months)*** | *5.5-21* | *1.5-10* | *3.9-6.3* | *20-100* | *5-21* | *13.5-21.5* | *150-550* |
| ***Control values Adults (> 7 year)*** | *4.5-13.5* | *1.5-8.5* | *4-5.2* | *20-100* | *5-21* | *11.5-15.5* | *150-450* |
| ***Control values Children*** | *5.5-15.5* | *1.5-8.5* | *3.9-5.3* | *20-100* | *5-21* | *11.5-13.5* | *150-550* |
| **Father** | 5.9 | 3.21 | 4.88 | ND | ND | 15.5 | 258 |
| **Mother** | 5.22 | 2.94 | 4.25 | ND | ND | 12.8 | 415 |
| **Healthy brother, 4 years** | 5.04 | 1.59 | 3.94 | ND | ND | 11.5 | 521 |
| **Propositus, 4 months** | 11.3 | 5.9 | **3.8** | **19** | ND | **10.6** | **65** |
| **Propositus, 1 years** | 8.85 | 3.8 | 3.91 | 45 | 18.2 | **10.0** | **65** |
| **Propositus, 2 years** | 10.98 | 4.7 | 3.94 | 43 | **25.4** | **10.2** | **64** |
| **Propositus, 3 years** | 10.22 | 3.3 | **3.78** | 39 | **27.2** | **10.3** | **60** |
| **Propositus, 4 years** | 7.84 | 3.9 | **3.41** | 27 | **39.3** | **9.1** | **9** |
| **Propositus, 5 years** | 14.53 | 9.7 | **3.69** | 56 | **32** | **10.7** | **41** |
| **Propositus, 6 years** | 7.61 | 2.9 | **3.77** | **14** | **22.2** | **10.6** | **15** |
| **Propositus, 8 years** | 7.06 | 3 | 4.67 | 25 | 7.8 | 13.6 | **77** |
| **Propositus, 8.5 years** | 9.49 | 4.4 | 4.24 | 37 | 9.7 | 12.5 | 152 |
| **Propositus, 9 years** | 7.89 | 3.9 | 4.2 | 36 | 10.6 | 12.5 | **132** |
| **Propositus, 9.5 years** | 9.97 | 5.6 | 4.72 | 40 | 10.4 | 13.4 | **113** |
| **Affected Sister, 1 week** | 11.64 | 3.4 | 5.73 | 25 | 16.1 | 19.1 | **73** |
| **Affected Sister, 5 months** | 9.34 | 2.2 | **3.33** | 45 | **24.7** | **8.6** | **148** |
| **Affected Sister, 7 months** | 10.15 | 3.8 | **3.2** | 34 | **22.2** | **7.8** | **124** |
| **Affected Sister, 9 months** | 13.18 | 5.5 | **3.2** | 72 | **32.1** | **7.7** | **107** |
| **Affected Sister, 1 year** | 14.58 | 4.1 | **2.67** | 76 | **41.6** | **6.3** | **24** |

(B) Serial assessments of peripheral blood films and bone marrow biopsies in the propositus.

| | **Peripheral blood smears** | **Bone marrow biopsy** | **Bone marrow genetics** |
|---|---|---|---|
| II:2 (Propositus) 4 years | White blood cells normal, mild normocytic normochromic anemia with mild aniso-poikilocytosis and severe thrombocytopenia. | Erythrophagocytosis. Dysplastic megakaryocytes that are located in clusters. Normal lymphoid lineage with granulocytes. Myelofibrosis grade 2 reticulin staining. | Negative: BCR-ABL, FISH (monosomy 7), JAK2, CALR and MPL, chromosomal breakage |
| II:2 (Propositus) 5 years | Mild monocytosis and neutrophilia , mild normocytic normochromic anemia with anisopoikilocytosis and obvious thrombocytopenia | Left-shifted myeloid lineage. Increased numbers of dysplastic megakaryocytes. Erythroid lineage difficult to study due to insufficient numbers. Myelofibrosis grade 3. Cellularity 90%, myeloid/erythroid: 4/1. | |
| II:2 (Propositus) 8 years | Mild poikilocytosis and thrombocytopenia. | Normal cellularity 70-80%. Normocellular but hyperplastic and left-shifted myeloid lineage. Prominent hyperplastic megakaryocyte lineage with strong cluster formation on LAT staining. Megakaryocyte dysplasia with both hyperlobulated and small hypolobulated, hyperchromic cells. Normocellular erythroid lineage without dysplasia. Myelofibrosis grade 3. Mason trichrome staining of bone marrow showed mature collagen fibers (grade 3). | Negative: NGS panel test TruSight Myeloid Sequencing (Illumina) with coverage of 500x. FISH with normal karyotype. |

(C) Platelet light transmission aggregometry studies.

The propositus had normal aggregation responses for ristocetin (105%), arachidonic acid (95%), U46619 (111%), collagen at 2 μg/ml (70%) and ADP at 5 μM (97%). Only the response to low dose of collagen was mildly reduced.

| | **Propositus*** | **Two unrelated healthy controls*** |
|---|---|---|
| Amplitude for Horm collagen 1μg/ml | 25% | 63 and 66% |
| Amplitude for ADP 2.5 μM | 52% | 48 and 28% |

*All aggregations were performed using platelet-rich plasma at $90x10^3$ platelets/μL.

**Supplemental Table 2**

**Ion counts from Metabolon analysis of plasma sphingolipids from the propositus, healthy brother, parents, and 496 unrelated controls.**

3-ketosphinganine (KDS) was detectable in only the propositus. Downstream metabolites were not reduced, and the enzymatic product of KDSR dihydrosphingosine (DHS) was in fact unexpectedly high. NF, not found

| | Propositus | Healthy brother | Mother | Father | Median (controls) | S.D (controls) |
|---|---|---|---|---|---|---|
| KDS | 8.5 E5 | NF | NF | NF | NF | NF |
| DHS | 3.6 E5 | NF | NF | NF | 6.7 E4 | 3.2 E4 |
| Dihydroceramide | 6.3 E5 | 2.5 E5 | 3.3 E5 | 2.6 E5 | 3.1 E5 | 1.8 E5 |
| Sphinganine-1-phosphate | 6.7 E5 | 4.0 E5 | 4.6 E5 | 3.4 E5 | 3.9 E5 | 1.4 E5 |
| Ceramide | 3.5 E6 | 2.8 E6 | 3.6 E6 | 2.9 E6 | 2.8 E6 | 7.9 E6 |
| Sphingosine | 1.8 E5 | 9.5 E4 | 1.0 E5 | 6.2 E4 | 1.5 E5 | 8.3 E4 |
| Sphingosine 1-phosphate | 3.4 E6 | 2.7 E6 | 3.1 E6 | 2.3 E6 | 2.6 E6 | 6.2 E5 |
| Total sphingomyelins | 1.3 E9 | 1.2 E9 | 1.2 E9 | 1.3 E9 | 1.2 E9 | 1.8 E8 |
| Total glycosphingolipids | 1.2 E7 | 1.2 E7 | 8.9 E7 | 1.2 E7 | 1.0 E7 | 2.6 E6 |
| Phosphoethanolamine | 1.6 E6 | 1.7 E6 | 1.1 E6 | 8.0 E5 | 1.6 E6 | 6.1 E5 |

**Supplemental Table 3**

**Ion counts from targeted sphingolipid analysis by LC-MS**

(A) Plasma sphingolipid analysis by LC-MS. Metabolites downstream of KDSR were not reduced in affected individuals (propositus, affected sister) compared with unaffected individuals (healthy brother, parents and controls). DHS, sphingosine and S1P are not measurable by this method. Differences were analyzed using the paired, two-tailed Student's *t*-test, using $p<0.05$ for significance.

| Plasma | Propositus | Affected Sister | Healthy Brother | Mother | Father | Control 1 | Control 2 | *p* |
|---|---|---|---|---|---|---|---|---|
| Dihydroceramides | 3.78E-3 | 6.06E-3 | 3.90E-3 | 3.21E-3 | 2.60E-3 | 2.34E-3 | 8.46E-3 | 0.52 |
| Ceramides | 2.34E-2 | 8.70E-3 | 7.21E-3 | 6.48E-3 | 8.66E-3 | 5.64E-3 | 1.37E-2 | 0.5 |
| Glycosphingolipids | 1.78E-3 | 1.05E-3 | 1.69E-3 | 1.85E-3 | 1.98E-3 | 1.64E-3 | 4.04E-3 | 0.56 |
| Sphingomyelins | 11.7 | 5.26 | 9.31 | 9.01 | 11.3 | 4.17 | 11.5 | 0.74 |

(B) Analysis of zebrafish protein lysates by LC-MS. Metabolites downstream of Kdsr were not significantly different between *kdsr*-ATG morpholino targeted fish (800μM) and controls. Differences were analyzed using the paired, two-tailed *t*-test, using $p<0.05$ for significance.

| Zebrafish protein lysate | Control 1 | Control 2 | Control 3 | *kdsr*-ATG 1 | *kdsr*-ATG 2 | *kdsr*-ATG 3 | *p* |
|---|---|---|---|---|---|---|---|
| Dihydroceramides | 1.02 E3 | 2.31 E3 | 8.31 E4 | 5.98 E4 | 3.26 E4 | 5.23 E4 | 0.16 |
| Ceramides | 3.67 E3 | 9.43 E3 | 3.07 E3 | 3.43 E3 | 1.46 E3 | 3.82 E3 | 0.33 |
| Glycosphingolipids | 5.11 E5 | 0.00 | 4.40 E5 | 3.26 E5 | 5.28 E5 | 1.01 E4 | 0.19 |
| Sphingomyelins | 2.05 | 2.06 | 2.02 | 2.06 | 1.64 | 2.34 | 0.91 |

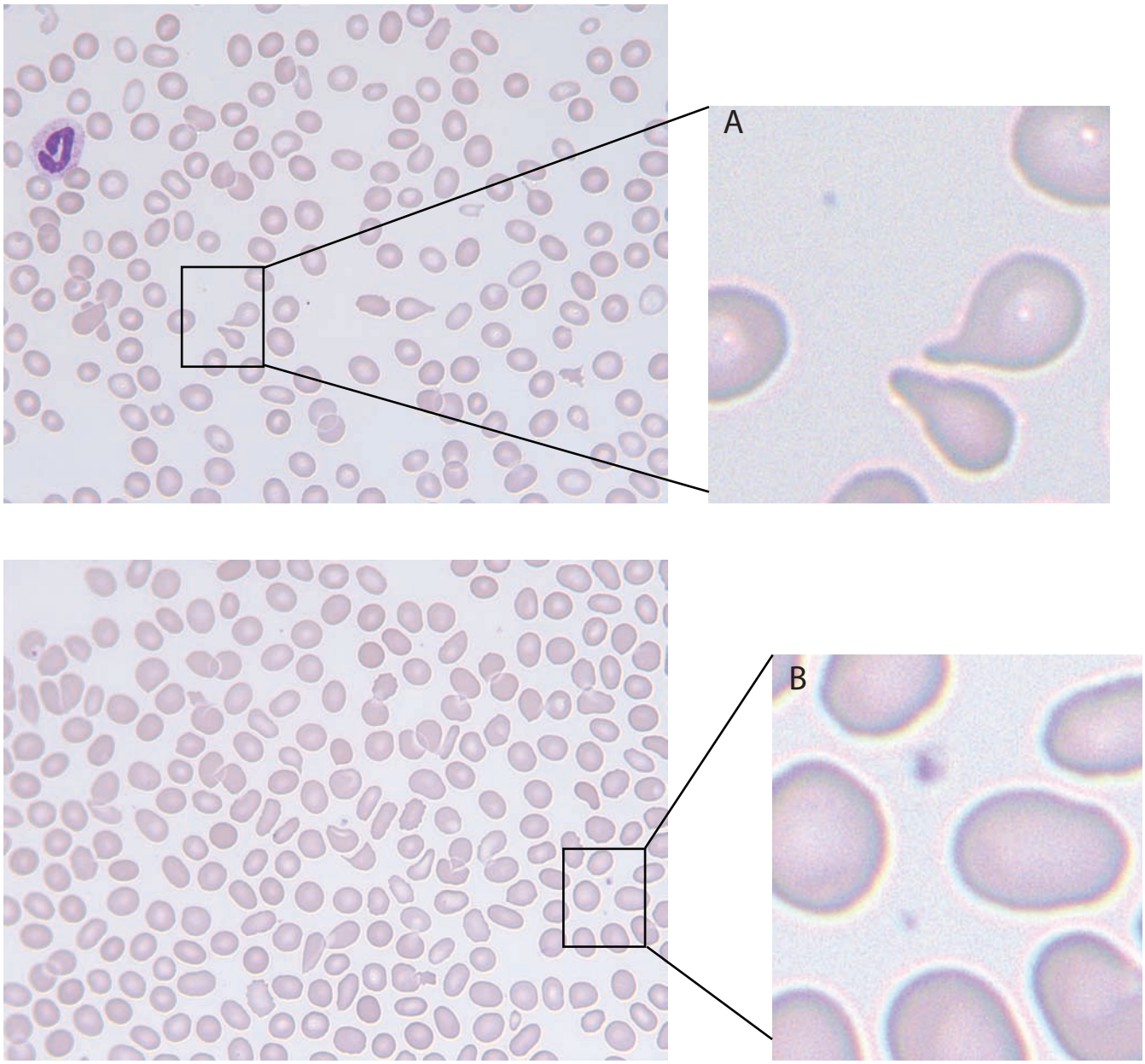


**Supplemental Figure 1**
**Peripheral blood smears from the propositus taken at 6 years of age**
Dysmorphic erythrocytes with poikilocytosis including (A) tear drop cells and (B) thrombocytopenia with platelets of normal volume are shown (magnification x100).

A

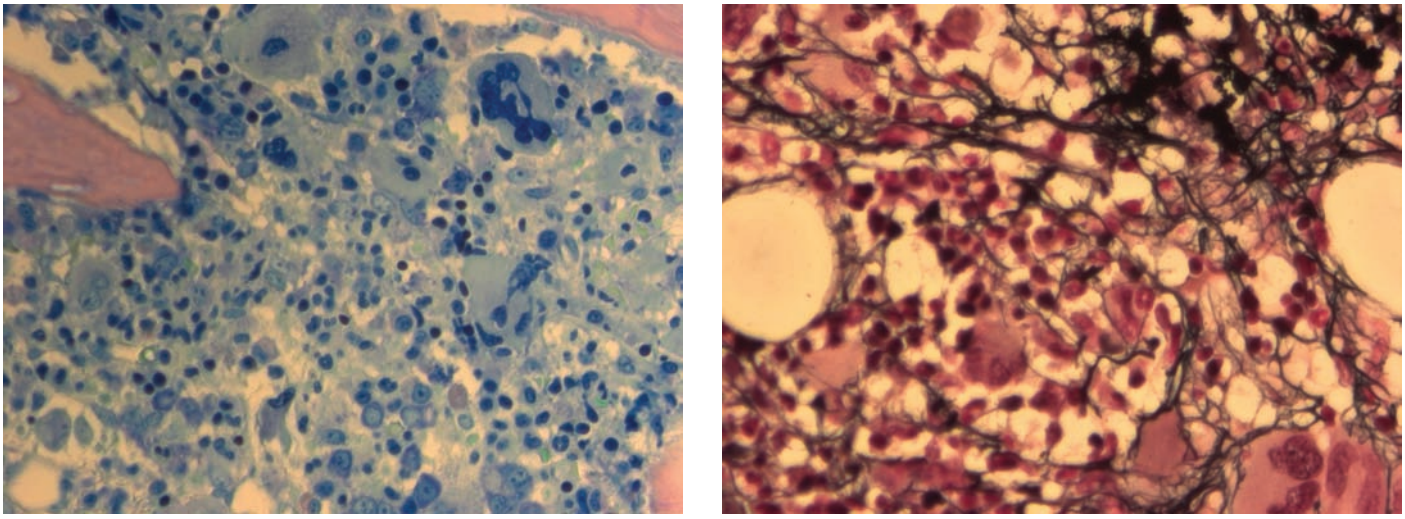

B

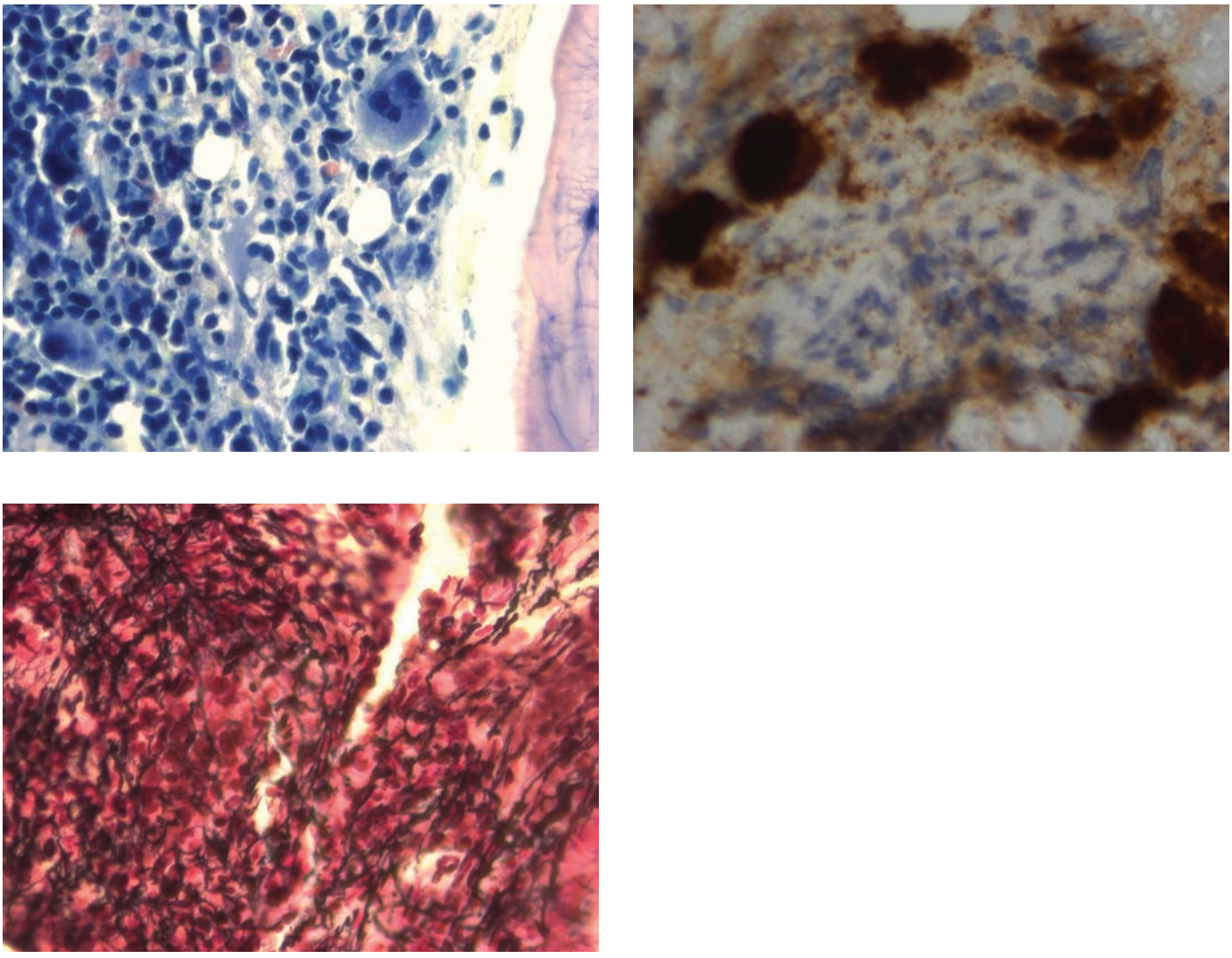

**Supplemental Figure 2**
**Bone marrow (BM) biopsies from the propositus**
(A) BM biopsy at 4 years of age. Left: Dysplastic megakaryocytes (MK) forming unusually large clusters. Right: Fibrosis with reticulin staining. (B) BM biopsy at 8 years of age. Left and right upper: Dysplastic MK in clusters. Left lower: Marrow fibrosis with strong stromal reticulin staining (magnification x40).

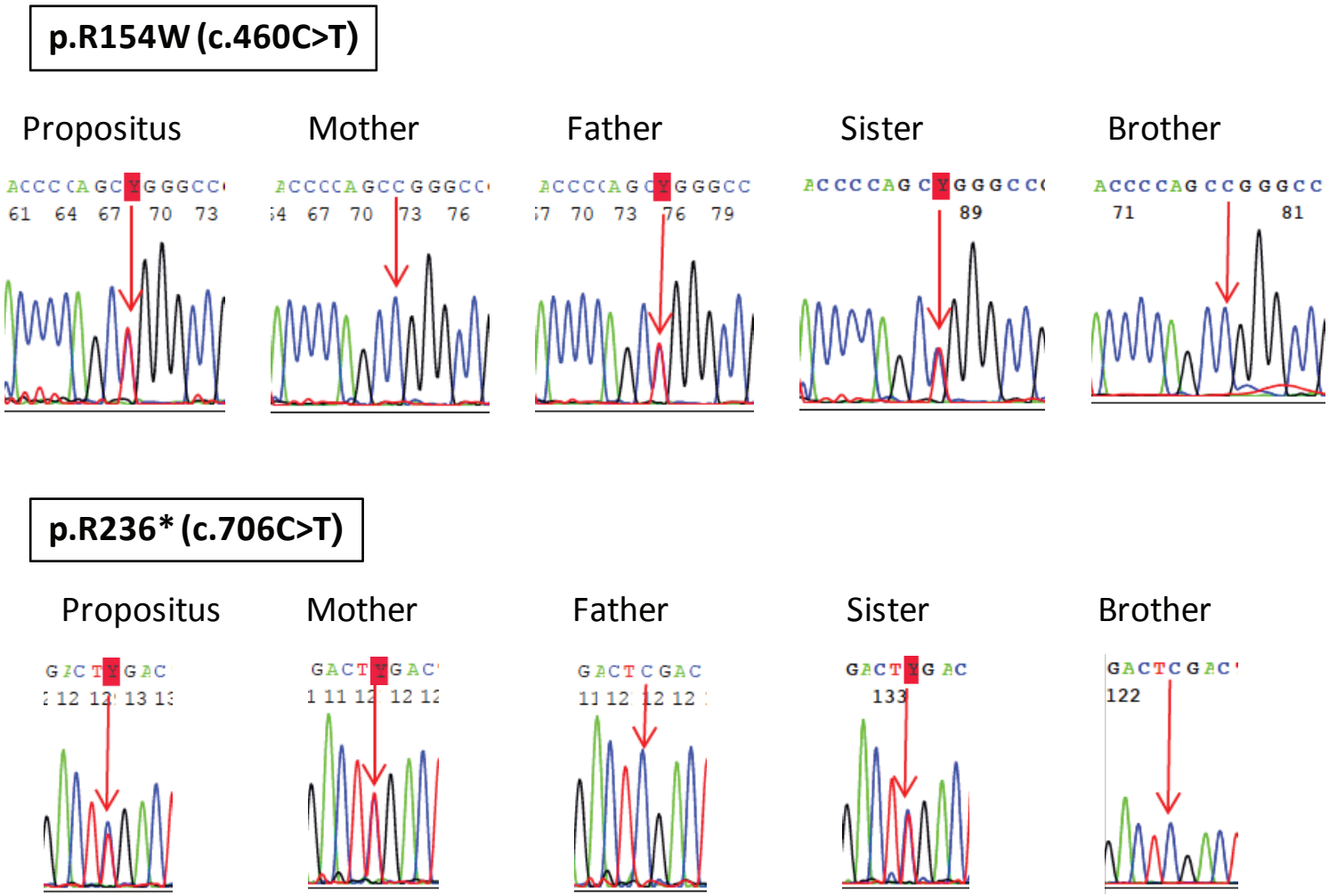


**Supplemental Figure 3**
**Sanger sequencing confirms putative pathogenic *KDSR* variants**
Two rare variants (18:61006104 G>A and 18:61018270 G>A) were confirmed by Sanger sequencing in the proband and his affected sister. The healthy brother carried the major allele for both variants.

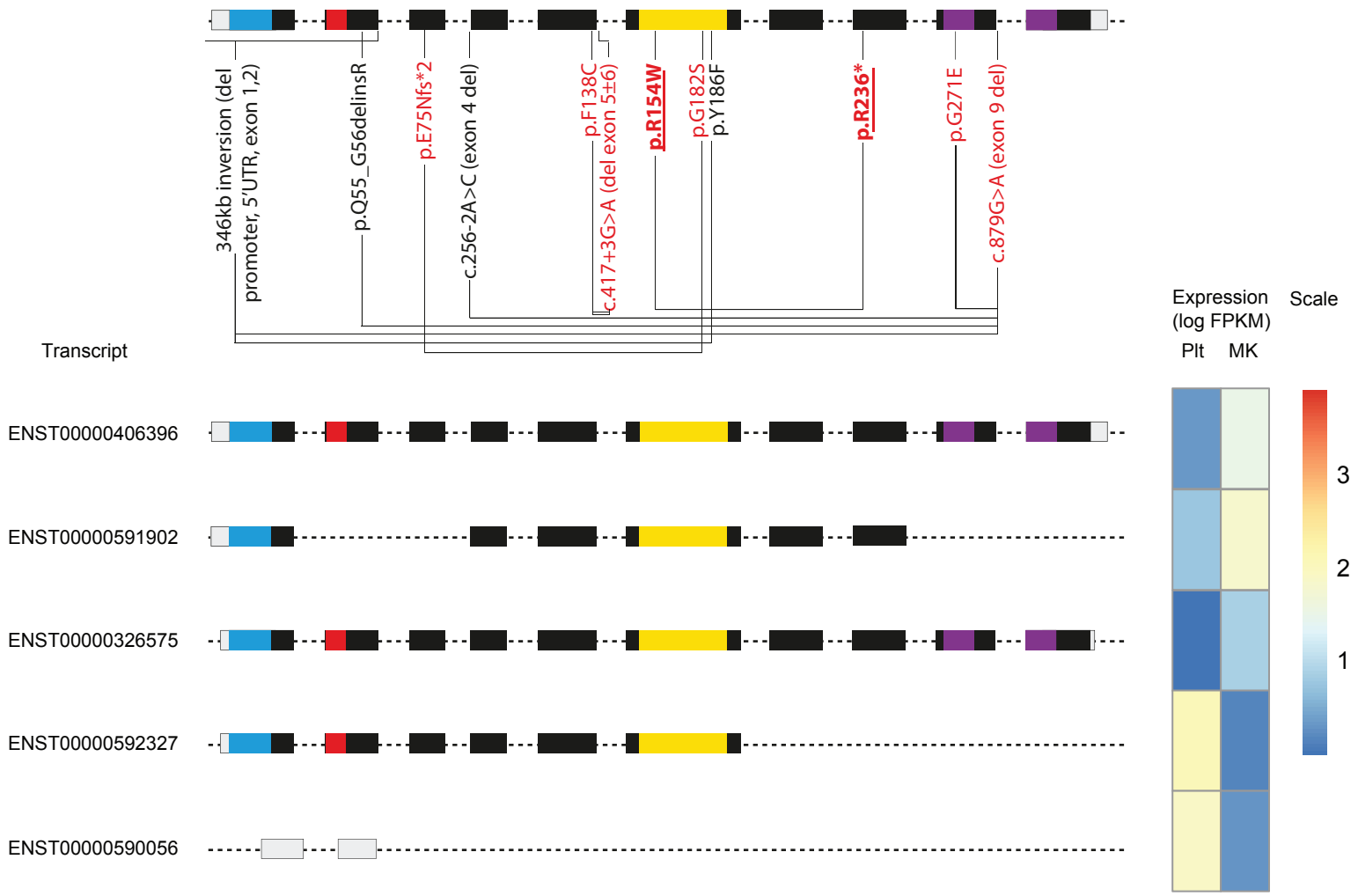


**Supplemental Figure 4**

**Heatmap of *KDSR* transcripts in MK and platelets (Plt)**

Transcripts present at >0·5 log FPKM (fragments per kilobase of transcript per million mapped reads) are shown and schematically represented. Key structural elements and variant annotation are as defined in Figure 1. The variants present in the affected siblings are highlighted in bold, and are present in the major transcripts present in MK (ENST00000406396, ENST00000591902) but not platelets (ENST00000592327, ENST00000590056, http://blueprint.haem.cam.ac.uk).[8] This is in keeping with previous reports that de novo sphingolipid synthesis plays a minimal role in mature platelets.[9]

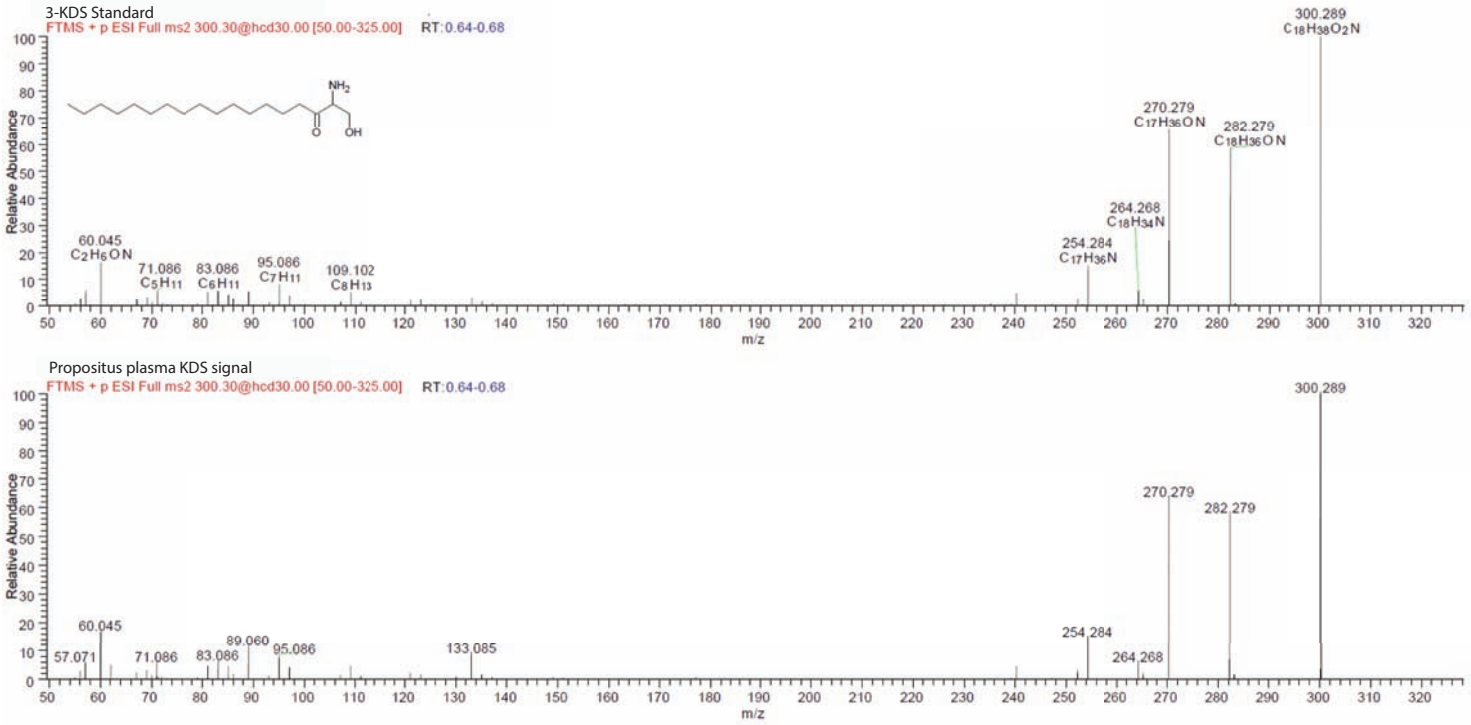


**Supplemental Figure 5**

**Mass spectrum of 3-KDS in propositus and standard**

An LC-MS platform was used to confirm the metabolic phenotype in the propositus and affected sister. The MS2 spectrum is shown for the 3-KDS biochemical standard and the propositus, showing conformity of peaks. FTMS, Fourier transformation mass spectrometry; +pESI, positive mode electrospray ionisation; HCD, higher energy collisional dissociation. Set at the specific fragmentation of ion 300·3 m/z by HCD at a relative energy of 30%, obtaining data from the range 50 to 325 m/z.

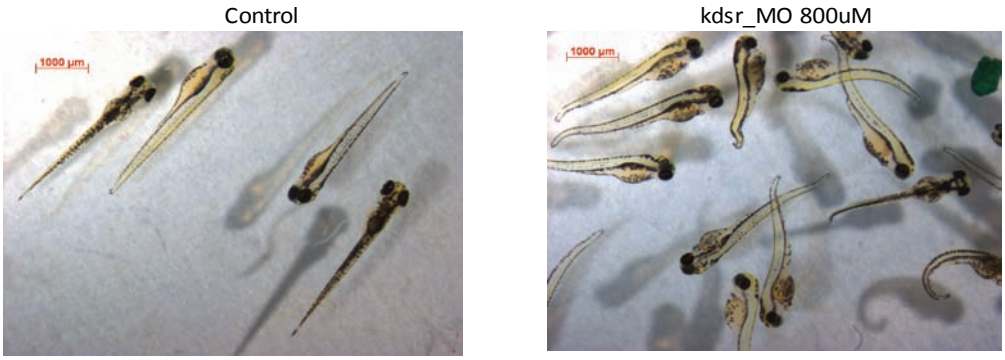


**Supplemental Figure 6**
**Zebrafish experiments**
Tg(cd41:EGF) embryos were injected with a kdsr ATG-MO (1000 µM) or with buffer (control). At 72 hpf most embryos developed curled tails but no other dysmorphisms.

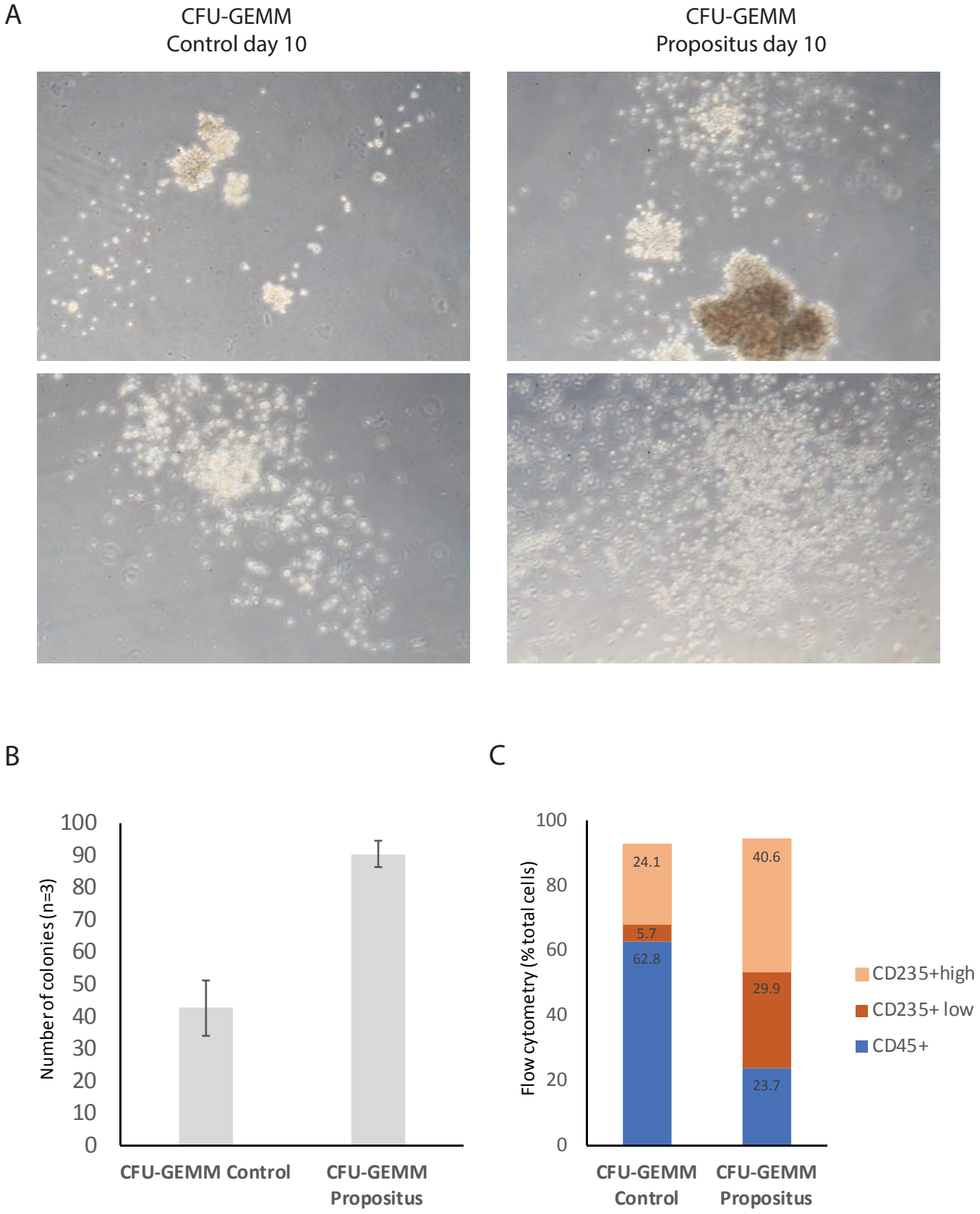


**Supplemental Figure 7**
**Myeloid stem cell differentiation assays from propositus at 5 years of age**
(A, B) Representative images of CFU-GEMM colonies counted at day 10 of differentiation of CD34+ bone-marrow HSC. There was a higher number and increased density of colonies for the propositus compared with controls. Means and standard deviations of three experiments are shown. (C) Flow cytometry analysis following staining with anti-CD45 and anti-CD235 antibodies to stain the myeloid and erythroid lineage, respectively. The proportion of myeloid leukocytes was higher in control cultures, whilst cultures from the propositus were enriched for erythroid progenitors.

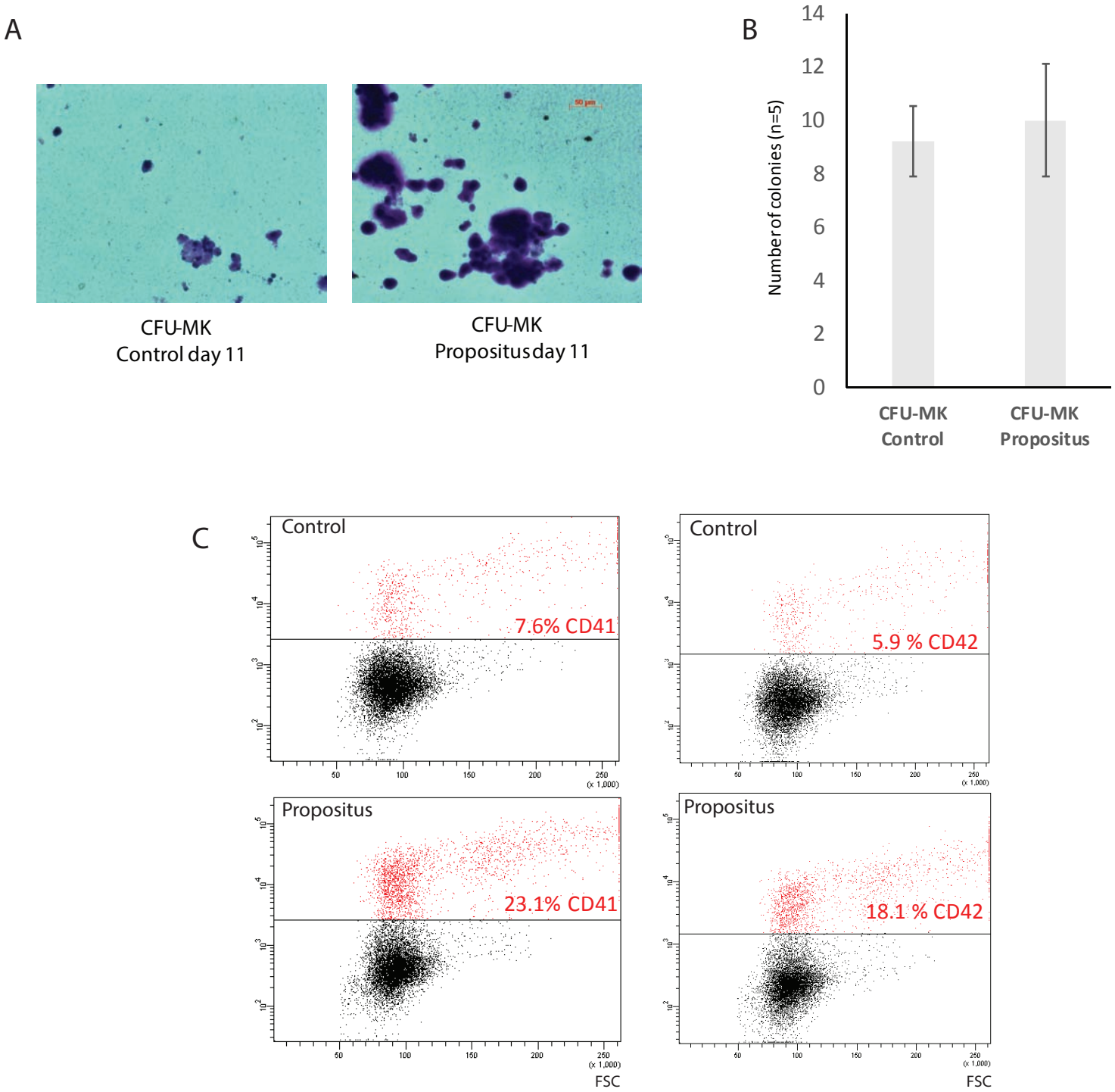


**Supplemental Figure 8**
**Megakaryocyte colony assays**
(A) MegaCult cultures. Representative images of CFU-MK colonies at day 11 of differentiation of CD34+ bone-marrow HSC. We observed an increased density of colonies for the propositus compared with controls. (B) However the total number of MK colonies was comparable between conditions. Means and standard deviations of 5 experiments are shown. (C) Liquid MK cultures were analysed at day 7 of differentiation using flow cytometry. A higher number of cells expressed mature MK markers CD41 and CD42 in cultures derived from the propositus compared with controls. FSC, forward scatter.

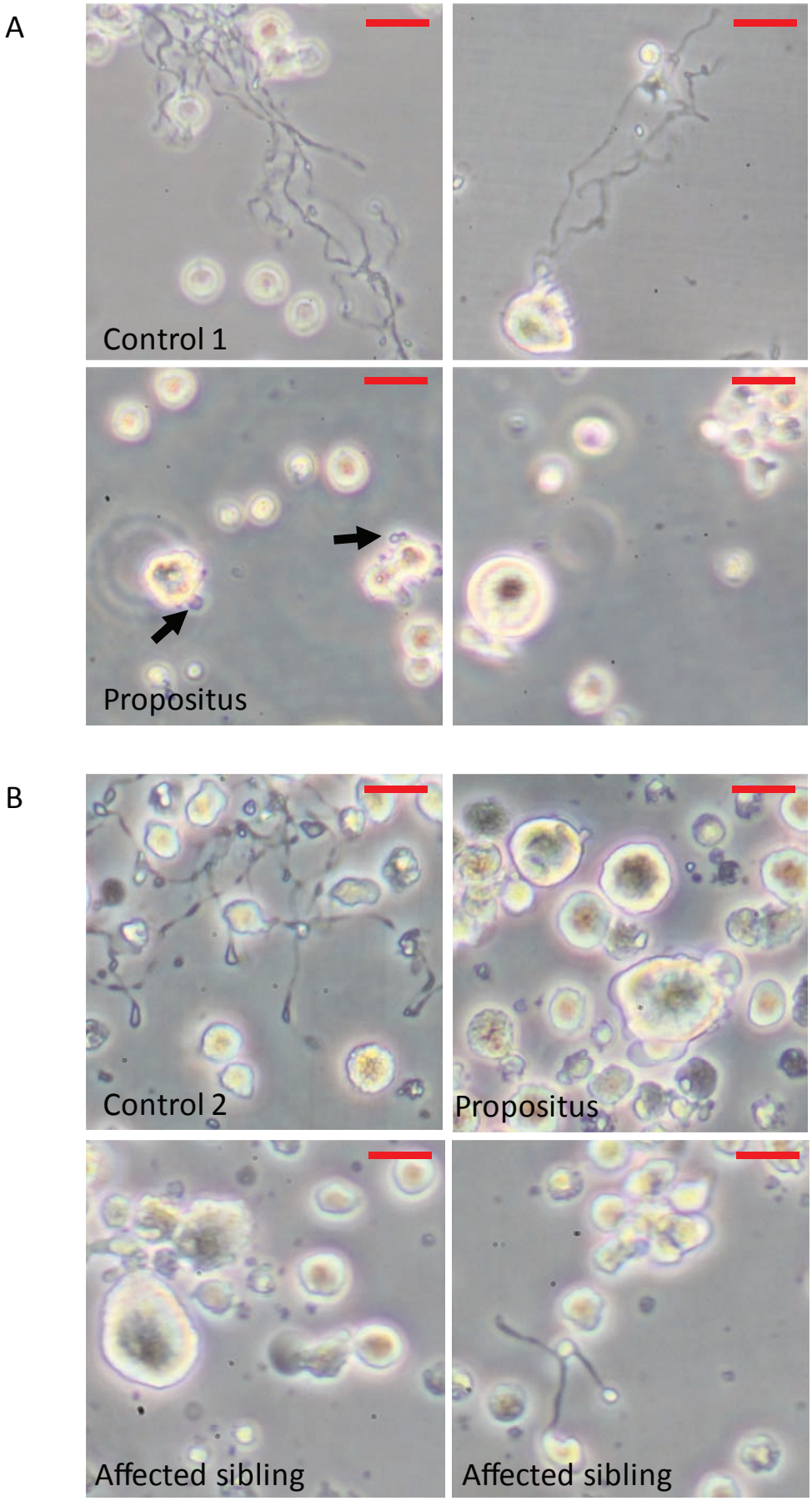


**Supplemental Figure 9**
**Liquid megakaryocyte cultures show impaired proplatelet formation**
(A) MK proplatelet formation was measured at day 11 of differentiation using bone marrow-derived CD34+ HSC from the propositus and controls. Propositus-derived MK were unusually large and displayed reduced proplatelet formation. (B) MK proplatelet formation was measured at day 12 of differentiation using peripheral blood derived CD34+ HSC from the propositus and affected sister. Again, MK from the patients were large and displayed membrane budding (arrows) but did not form normal proplatelets. Scale bars indicate 50 μm.

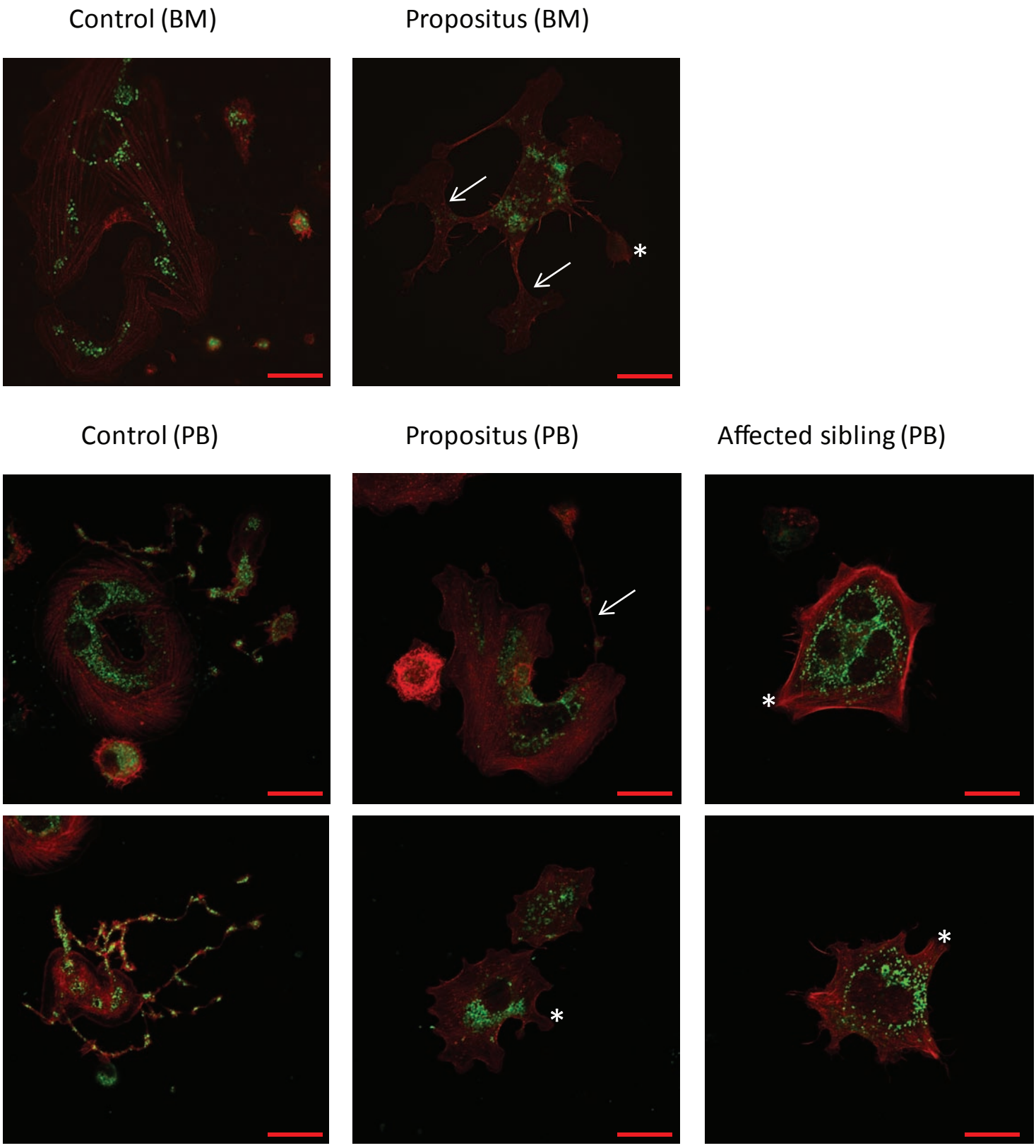


**Supplemental Figure 10**
**Immunostaining of CD34+ stem cell-derived megakaryocytes confirm impaired proplatelet formation, and show abnormal cytoskeletal organisation**
Megakaryocytes derived from bone marrow (BM) or peripheral blood (PB) were spread on fibrinogen and immunostained with antibodies against cytoskeletal marker F-actin (red) and δ-granule marker CD63 (green). MK for the propositus and his affected sibling showed irregular cytoskeletal structures that resembled filopodia (*). Proplatelet formation was infrequent and observed proplatelets demonstrated reduced δ-granule trafficking (arrow). Scale bars indicate 20μm.

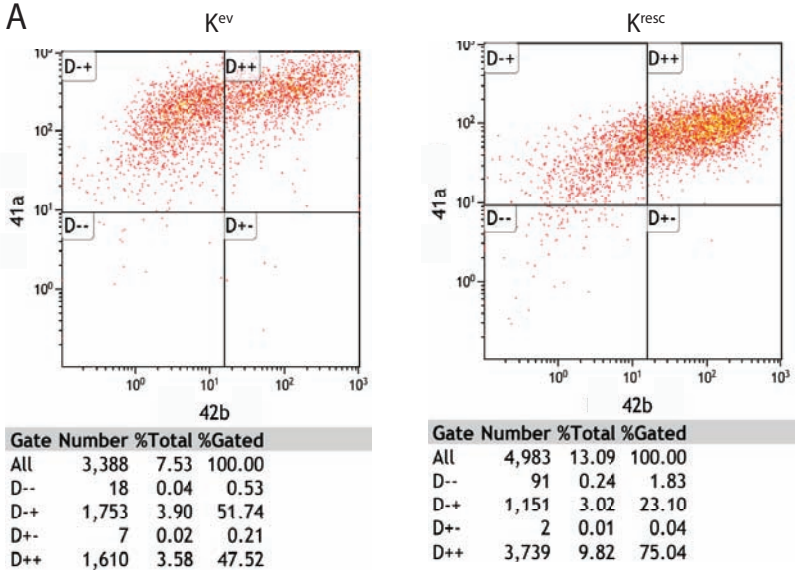


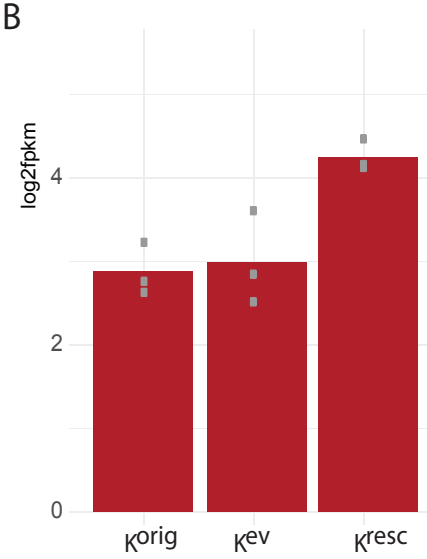


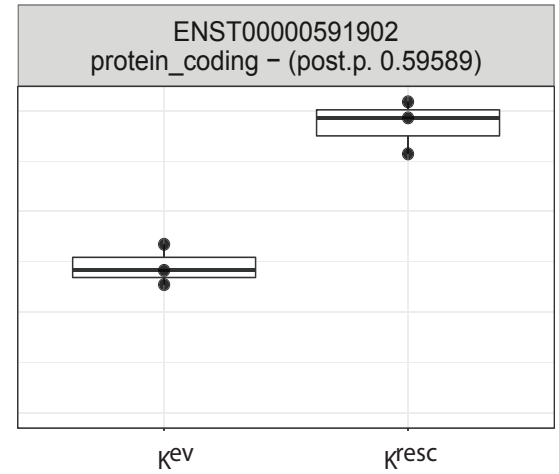


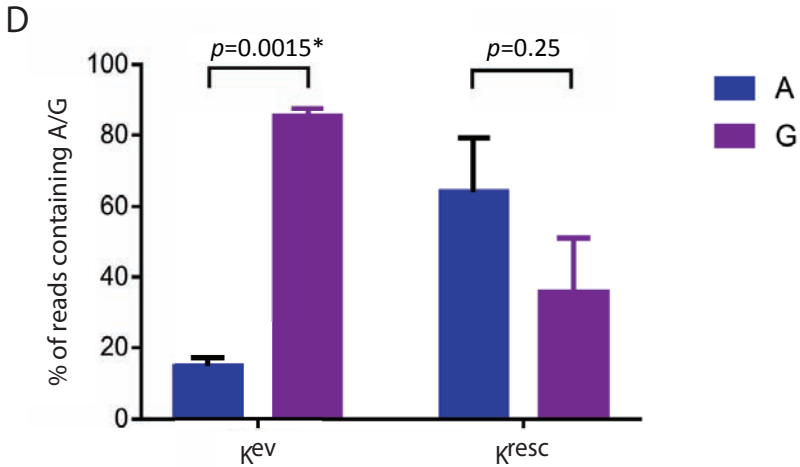


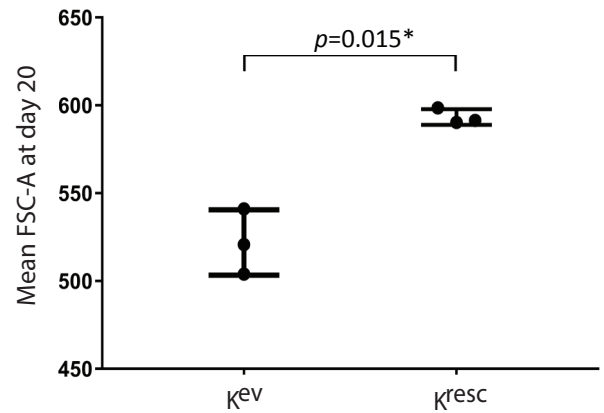


**Supplemental Figure 11**

**Gene expression analysis by RNA-seq in $K^{resc}$ and $K^{ev}$ iMK is consistent with correction of the genetic defect, without significant overexpression**

(A) iPSC from the propositus were transduced with lentiviral vectors containing the reference *KDSR* ORF ($K^{resc}$) or an inert control ($K^{ev}$), then reprogrammed to iMK. Single, viable cells were assessed by flow cytometry for markers of iMK at day 20 of forward programming. In both conditions the majority of cells were CD41+ and CD42+, in keeping with differentiation to iMK. (B) *KDSR* expression was assessed by RNA-seq. At the gene level there was no significant difference in normalised *KDSR* expression between propositus-derived iMK ($K^{orig}$), $K^{ev}$ and $K^{resc}$ iMK. (C) At the transcript level ENST00000591902 was differentially expressed and higher in $K^{resc}$ iMK. This transcript corresponds to the *KDSR* sequence in the wild-type expression vector and is the transcript with the highest expression in MK.[8] A posterior probability of differential expression > 0·5 was considered significant. (D) $K^{resc}$ iMK carried the reference allele at Chr18:61018270 G>A (p.Arg154Trp) (mean count G: 192 (84%), A: 36 (16%), $p = 0{\cdot}0015$ by paired, two-tailed *t*-test). $K^{ev}$ iMK expression was consistent with heterozygosity (mean count G: 14 (33%), A: 29 (67%), $p = 0{\cdot}25$). Values plotted are mean number of transcripts and error bars show the standard deviation, across three independent experiments. (E) iMK were defined by flow cytometry as CD41+ viable, single cells and forward scatter area (FSC-A) was measured for each experimental replicate. The means and standard deviations of FSC-A are plotted for the three experimental replicates. At day 20 $K^{resc}$ iMK were significantly larger than $K^{ev}$ iMK ($p = 0{\cdot}015$ by paired, two-tailed *t*-test).

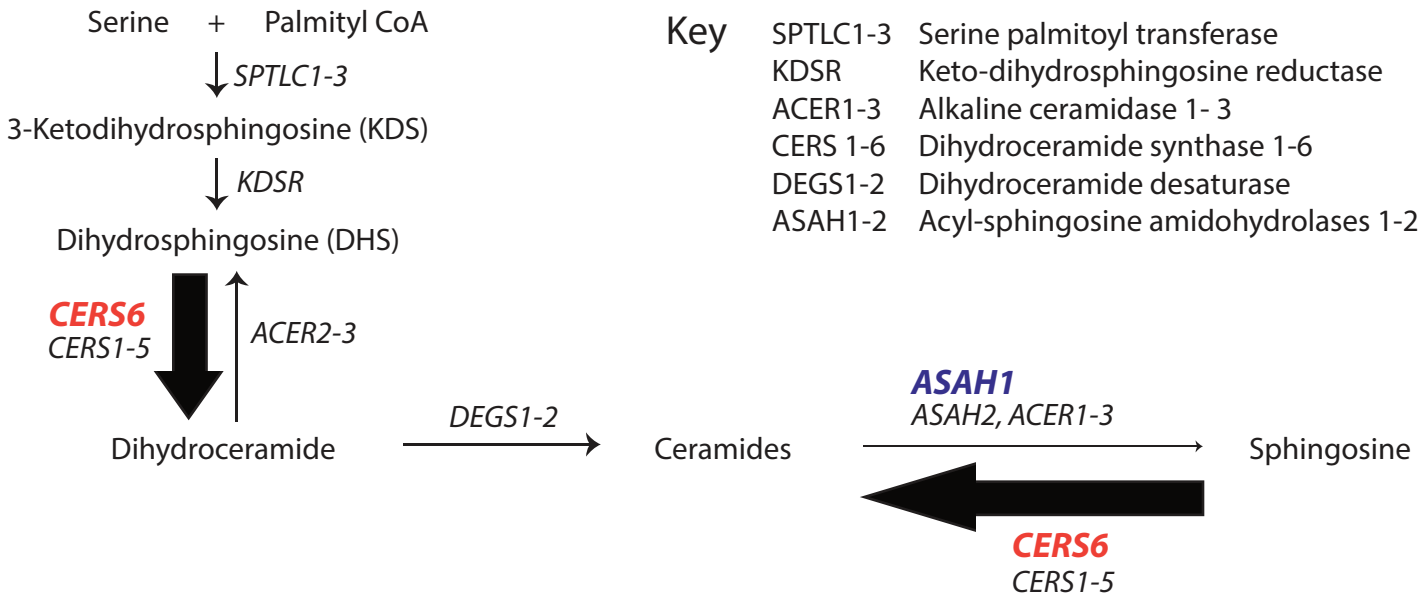


**Supplemental Figure 12**
**Differential expression of ASAH1 and CERS6 between Kresc and Kev suggests that KDSR variants result in ceramide and sphingosine imbalance**
Gene expression was assessed by RNA-seq. Using a posterior probability of differential expression > 0.5 for significance, only two of the sphingolipid enzymes listed in Figure 4A were significantly differentially expressed between $K^{resc}$ and $K^{ev}$. ASAH1 (posterior probability = 0·61, estimated log fold change = -0·67) was down-regulated in the $K^{ev}$ condition and CERS6 (posterior probability = 0·774, estimated log fold change = +0·70) was up-regulated in the $K^{ev}$ condition. *ASAH1* and *CERS6* act in opposition to regulate the balance between ceramide and sphingosine. These findings are in keeping with the metabolic profile of higher sphingosine and lower ceramide in $K^{resc}$ iMK compared with $K^{ev}$ iMK shown in Figure 7.

**Supplemental References**


1. Westbury SK, Turro E, Greene D, Lentaigne C, Kelly AM, Bariana TK, et al. Human phenotype ontology annotation and cluster analysis to unravel genetic defects in 707 cases with unexplained bleeding and platelet disorders. Genome medicine. 2015; **7**(1): 36.
2. Schindelin J, Arganda-Carreras I, Frise E, Kaynig V, Longair M, Pietzsch T, et al. Fiji: an open-source platform for biological-image analysis. Nature methods. 2012; **9**(7): 676-82.
3. Westmoreland D, Shaw M, Grimes W, Metcalf DJ, Burden JJ, Gomez K, et al. Super-resolution microscopy as a potential approach to diagnosis of platelet granule disorders. J Thromb Haemost. 2016; **14**(4): 839-49.
4. Louwette S, Regal L, Wittevrongel C, Thys C, Vandeweeghde G, Decuyper E, et al. NPC1 defect results in abnormal platelet formation and function: studies in Niemann-Pick disease type C1 patients and zebrafish. Human molecular genetics. 2013; **22**(1): 61-73.
5. Freson K, Peeters K, De Vos R, Wittevrongel C, Thys C, Hoylaerts MF, et al. PACAP and its receptor VPAC1 regulate megakaryocyte maturation: therapeutic implications. Blood. 2008; **111**(4): 1885-93.
6. Turro E, Greene D, Wijgaerts A, Thys C, Lentaigne C, Bariana TK, et al. A dominant gain-of-function mutation in universal tyrosine kinase SRC causes thrombocytopenia, myelofibrosis, bleeding, and bone pathologies. Science translational medicine. 2016; **8**(328): 328ra30.
7. Heremans J, Garcia-Perez JE, Turro E, Schlenner SM, Casteels I, Collin R, et al. Abnormal differentiation of B cells and megakaryocytes in patients with Roifman syndrome. The Journal of allergy and clinical immunology. 2018.
8. Takahashi K, Tanabe K, Ohnuki M, Narita M, Ichisaka T, Tomoda K, et al. Induction of pluripotent stem cells from adult human fibroblasts by defined factors. Cell. 2007; **131**(5): 861-72.
9. Yu J, Vodyanik MA, Smuga-Otto K, Antosiewicz-Bourget J, Frane JL, Tian S, et al. Induced pluripotent stem cell lines derived from human somatic cells. Science. 2007; **318**(5858): 1917-20.
10. Moreau T, Evans AL, Vasquez L, Tijssen MR, Yan Y, Trotter MW, et al. Large-scale production of megakaryocytes from human pluripotent stem cells by chemically defined forward programming. Nature communications. 2016; **7**: 11208.
11. Dobin A, Davis CA, Schlesinger F, Drenkow J, Zaleski C, Jha S, et al. STAR: ultrafast universal RNA-seq aligner. Bioinformatics. 2013; **29**(1): 15-21.
12. Liao Y, Smyth GK, Shi W. featureCounts: an efficient general purpose program for assigning sequence reads to genomic features. Bioinformatics. 2014; **30**(7): 923-30.
13. Turro E, Astle WJ, Tavare S. Flexible analysis of RNA-seq data using mixed effects models. Bioinformatics. 2014; **30**(2): 180-8.
14. Turro E, Su SY, Goncalves A, Coin LJ, Richardson S, Lewin A. Haplotype and isoform specific expression estimation using multi-mapping RNA-seq reads. Genome biology. 2011; **12**(2): R13.
15. Chen L, Kostadima M, Martens JH, Canu G, Garcia SP, Turro E, et al. Transcriptional diversity during lineage commitment of human blood progenitors. Science. 2014; **345**(6204): 1251033.
16. Tani M, Sano T, Ito M, Igarashi Y. Mechanisms of sphingosine and sphingosine 1-phosphate generation in human platelets. Journal of lipid research. 2005; **46**(11): 2458-67.